Journal Pre-proof

Multiple thermochronometers applied to the quantitative analysis of compressive systems: The southern sub-Andean fold and thrust belt of Bolivia. From source rock to trap

Juan I. Hernandez, Roberto M. Hernandez, Alejandra Dalenz Farjat, Ernesto O. Cristallini, Luis A. Alvarez, Luis M. Dellmans, Marcos R. Costilla, Andres F. Alvarez, Raul Becchio, Sofia Bordese, Guadalupe Arzadun, Cristina Guibaldo, Ulrich A. Glasmacher, Renata N. Tomezzoli, Daniel F. Stockli, Facundo Fuentes, Jaime Soria Galvarro, Adolfo Rosales, Francisco Dzelalija, Claudio Haring

PII: S0895-9811(20)30492-2

DOI: https://doi.org/10.1016/j.jsames.2020.102949

Reference: SAMES 102949

To appear in: *Journal of South American Earth Sciences*

Received Date: 9 June 2020

Revised Date: 23 September 2020

Accepted Date: 6 October 2020

Please cite this article as: Hernandez, J.I., Hernandez, R.M., Farjat, A.D., Cristallini, E.O., Alvarez, L.A., Dellmans, L.M., Costilla, M.R., Alvarez, A.F., Becchio, R., Bordese, S., Arzadun, G., Guibaldo, C., Glasmacher, U.A., Tomezzoli, R.N., Stockli, D.F., Fuentes, F., Galvarro, J.S., Rosales, A., Dzelalija, F., Haring, C., Multiple thermochronometers applied to the quantitative analysis of compressive systems: The southern sub-Andean fold and thrust belt of Bolivia. From source rock to trap, *Journal of South American Earth Sciences* (2020), doi: https://doi.org/10.1016/j.jsames.2020.102949.

Multiple thermochronometers applied to the quantitative analysis of compressive systems: the southern sub-Andean fold and thrust belt of Bolivia. From source rock to trap

Author Statement

Juan I. Hernandez: Conceptualization, Writing-Original draft and revised version preparation and figures, reviewing-editing, Investigation, numerical modeling. Roberto M. Hernandez: Conceptualization, reviewing. Alejandra Dalenz Farjat: Conceptualization, reviewing. Ernesto O. Cristallini: Conceptualization, reviewing, cross section construction, Luis A. Alvarez: Conceptualization, field work and geology. Luis M. Dellmans: field work and geology, figures development. Marcos R. Costilla: Conceptualization, mapping. Andres F. Alvarez: field work and geology. Raul Becchio: analytical work. Sofia Bordese: methodology, analytical work and reviewing. Guadalupe Arzadun: analytical work. Cristina Guibaldo: analytical work. Ulrich A. Glasmacher: analytical work, methodology, reviewing and editing manuscript. Renata N. Tomezzoli: reviewing manuscript, methodology. Daniel F. Stockli: analytical work. Facundo Fuentes: geology, funding acquisition. Jaime Soria Galvarro: geology, funding acquisition. Adolfo Rosales: geology, funding acquisition. Francisco Dzelalija: funding acquisition. Claudio Haring: funding acquisition.

Multiple thermochronometers applied to the quantitative analysis of compressive systems: the southern sub-Andean fold and thrust belt of Bolivia. From source rock to trap

Juan I. Hernandez[1,2,*], Roberto M. Hernandez[1,2], Alejandra Dalenz Farjat[1], Ernesto O. Cristallini [2,3], Luis A. Alvarez[1], Luis M. Dellmans[1], Marcos R. Costilla[1], Andres F. Alvarez[1], Raul Becchio[2,4], Sofia Bordese[2], Guadalupe Arzadun[2], Cristina Guibaldo[2,5], Ulrich A. Glasmacher[6], Renata N. Tomezzoli[7], Daniel F. Stockli[8], Facundo Fuentes[9], Jaime Soria Galvarro[10], Adolfo Rosales[10], Francisco Dzelalija[9], Claudio Haring[9]

(1) GEOMAP, Av. Ricardo Durand N° 397, Salta, Argentina. E-mail: hernandezj@xrgeomap.net.
(2) LA.TE. ANDES S.A., Las Moreras 510, Vaqueros, Salta, Argentina. E-mail: hernandezj@lateandes.com.
(3) Instituto de Estudios Andinos "Don Pablo Groeber". IDEAN (CONICET-UBA).
(4) Instituto de Biología y Geología. IBIGEO (CONICET-UNSa).
(5) Comisión Nacional de Energía Atómica. CNEA. Argentina
(6) Institute of Earth Sciences, Heidelberg University. Germany.
(7) Instituto de Geociencias Básicas, Aplicadas y Ambientales de Buenos Aires. IGEBA (CONICET-UBA).
(8) Department of Geological Sciences, Jackson School of Geosciences, University of Texas at Austin, USA
(9) YPF S.A. Buenos Aires.
(10) YPFB Chaco S.A. Santa Cruz de la Sierra, Estado Plurinacional de Bolivia

*Corresponding author.
E-mail address: hernandezj@xrgeomap.net (J.I. Hernandez)

ABSTRACT

The evolution of fold and thrust belts requires time data restrictions to determine the rates related to the interaction of surface and subsurface processes and to quantify the time relationship between the components of the petroleum system: reservoir, seal, source rock and trap. The sub-Andean fold-and-thrust belt in the Bolivian territory in general, and the regional transect that links the structures of Curuyuqui-Carohuaicho-Tatarenda-Borebigua-Charagua and Mandeyapecua in particular, constitutes a complex multi-variable system in which the definition of time-Temperature (t-T) trajectories has led to new suitable structural and stratigraphic conclusions.

The integration of multiple thermochronological-geochronological systems (Apatite Fission Track, Apatite (U-Th-Sm)/He and UPb SHRIMP on zircon) and the existing surface and subsurface geological constraints made it possible to develop a chrono-kinematic characterization of fault-related anticlines, defining their formation chronology, structural growth rate and link between them in the study area. Furthermore, it was also possible to perform a quantitative analysis of the subsidence-burial and exhumation-erosion phenomena that occurred from the deposition of Silurian-Devonian source rocks to the present time, providing relevant determinations to the modeling of the Oil & Gas system.

Keywords: Thermochronology, geochronology, numerical modeling, quantitative analysis, sub-Andean fold and thrust belt, Bolivia, Andino 3D® software.

1. Introduction

The sub-Andean ranges of southern Bolivia and northwestern Argentina are a classic thin-skinned fold-and-thrust belt. They are bordered to the east by the Chaco Basin and by the inter-Andean system to the west (Fig. 1). The latter is defined to the west of the San Simon Frontal Thrusts, which is responsible for the inter-Andean uplift in Bolivia, while in Argentina it defines the Eastern Cordillera-sub-Andean border. This limit represents an important change with respect to the orography, structural style, and outcropping stratigraphic units (Kley et al., 1996). The inter-Andean–sub-Andean limit is due to a change in the main detachment level, from Ordovician-Silurian shales in the southern sub-Andean area to older basement units in the inter-Andean and Eastern Cordillera systems (Kley, 1996; Kley et al., 1996; Allmendinger and Zapata, 2000; Hernández et al., 2018).

The development of the fault-related anticlines in the sub-Andean fold-and-thrust belt of Bolivia and Argentina is controlled by vertical and horizontal anisotropies. In the vertical direction, the presence of different detachment ductile levels alternating with mechanically hard layers implied the division of the mechanical column into structural levels linked to one another, but with distinctive rheological characteristics.

To the south of 23°S latitude, the fold-and-thrust belt is superimposed over the Upper Cretaceous rift basin, developing some characteristics of thick-skinned deformation and tectonic inversion processes. In addition, the Cenozoic foreland basin infilling is partially controlled by inherited previous extensional structures (Allmendinger et al., 1983; Strecker et al., 1989; Hernández et al., 2005). Similar to the situation described by del Papa et al. (2013) for the Eastern Cordillera, the sub-Andean system to the south of 23° latitude behaves as a broken foreland basin (Kley and Monaldi, 2002; Hain et al., 2011; Siks and Horton, 2011; Strecker et al., 2012; Pearson et al., 2013), as opposed to the elastic beam of the classic foreland system defined by DeCelles and Giles (1996). In line with the latter, several authors have presented evidence aiming at a low broken foreland-component in northwestern Argentina (DeCelles et al., 2011; DeCelles et al., 2015; Engelder and Pelletier, 2015; Quade et al., 2015; Carrapa and DeCelles, 2015), which would resemble the scenario assumed for the study area.

The dynamics of both thin and thick-skinned deformation need time constraints in order to analyze the evolving scenarios, paying attention to the variables involved and the resulting stratigraphic and structural outputs. In line with this idea, the definition of statistically supported t-T paths in the southern sub-Andean system gave place to identifying heating and cooling phenomena not only related to the Miocene-to-Pliocene compressive stress field setting but also linked to *pre-Andean* processes, that is during Paleozoic and Mesozoic times. The combination of thermochronometers in order to define the thermal evolution attached to geological events represents the core-concept and main goal of the present study.

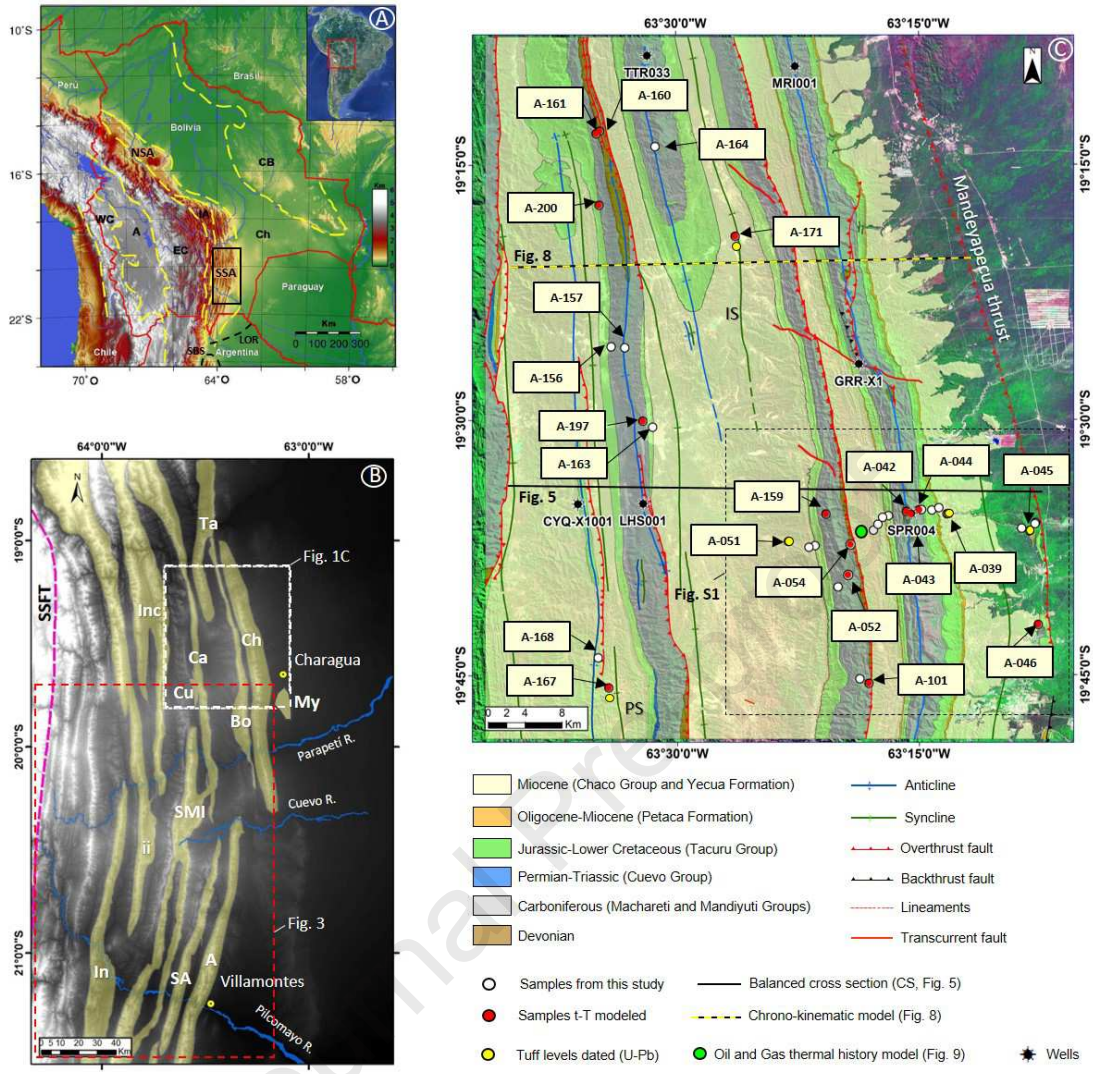

Fig.1. A. Digital elevation map with structural units defined in the central Andes. WC = Western Cordillera; A = Altiplano (Puna plateau); EC = Eastern Cordillera; IA = inter-Andean; NSA = Northern sub-Andean; SSA = Southern sub-Andean; Ch = Chaco Basin; CB = Brasilian Craton; LOR = Lomas de Olmedo Rift; SBS = Santa Bárbara System. Black square showing the area detailed in 1. B. B. Digital elevation model of southern sub-Andean system with ranges outlined. Ranges: A = Aguaragüe; Bo = Borebigua; Ca= Carohuaicho; Ch = Charagua; Cu = Curuyuqui; ii = Itacaray-Igüembe; In = Ingre; Inc = Incahuasi; My = Mandeyapecua; SA = San Antonio-San Alberto; SMI = Suaruro-Sararenda-Mandiyuti-Iñiguazu; Ta = Tatarenda. SSFT = San Simon Frontal Thrusts. Yellow points = main towns. Dotted white line square = study area (Fig. 1C). Dotted red line square = 3D sedimentary infilling model (according to Hernández et al., 2018; Fig. 3). C. Geological map of the study area, with structural cross-section location (black line, CS, Fig. 5) and chrono-kinematic model (black and yellow line, Fig. 8), and sample location (white dots). PS = Pirirenda Syncline, IS = Itai Syncline. Location of detailed geologic map in the Supplementary Information (SI) that shows individual sample numbers (Fig. S1) is denoted by box.

2. Geological setting

2.1. Structural framework. Mechanical stratigraphy

Hydrocarbon exploration in the sub-Andean fold-and-thrust belt in Argentina and Bolivia began at the beginning of the 20th century, with the development of simple and shallow anticline

models based on surface geology with Carboniferous targets located 700–900 m below ground surface. The need to incorporate liquid and gas hydrocarbon volumes in conventional reservoirs in the sub-Andean fold-and-thrust belt brought about exploration at greater depths (3,500–5,500 m). This in turn, led to additional reserves and a huge increase in knowledge about the deep structure.

The original definition of the southern sub-Andean thin-skinned fold-and-thrust belt in Bolivia and northwestern Argentina was presented by Mingramm and Russo (1969). According to their explanation, the general structure is formed by narrow outcropping anticlines with large strike-direction continuity, limited by broad and deep longitudinal synclines with a Silurian basal detachment level. It was also Mingramm and Russo (1969) who developed the first restorable cross-sections in the sub-Andean system, which allowed for the discovery of certain large deep gas fields in northwestern Argentina and southern Bolivia like Ramos, San Alberto, Aguaragüe, Bermejo and Macueta fields.

During the 1980s and 1990s, the exploration of the sub-Andean fold-and-thrust belt underwent a major drive through the construction of restorable structural cross-sections following geometric controls (Aramayo Flores, 1989; Baby et al., 1995; Dunn et al., 1995, among others), although neither the kinematic nor the mechanical properties of the rocks involved in the deformed stratigraphic column were strongly considered. These sections did not take into account the basement geometry related to pre-Andean deformation and accommodation processes, either.

Since the 2000s, the use and integration of analytical techniques linked to the resolution of both structural and stratigraphic problems in the sub-Andean system have increased their interest from both the applied and the scientific-academic point of view. In this sense, several and diverse analyzes were performed focusing on particular structures as well as on the dynamics and evolution of the sub-Andean system in an integral way, many of them aimed at characterizing the components and processes of the oil and gas systems. Among these studies linked to analytical techniques, the paleomagnetic determinations and absolute dating stand out (Hernández et al., 2002; Echavarría et al, 2003; Amidon et al., 2017; Uba et al., 2009), as well as the geochemical analyzes (Cruz et al., 2008; Schneider et al., 2018), the stable isotopes studies (Rosario et al., 2008, 2017; Mulch et al., 2010) and the thermochronological analyzes (Hernández et al, 2016, 2017; Anderson et al., 2018; Constantini et al, 2018).

In general, the frontal (eastern) flanks of the anticlines in the sub-Andean system are steep to overturned while the back (western) limbs show variable dip values from 30 degrees to almost vertical, even overturned (Hernández et al., 2002). Sometimes, the flanks of the structures exhibit dip variation along the strike, resulting in an apparent westward vergence in contrast to the general eastward direction of transport (e.g. Aguaragüe structure).

The deep structure is characterized by low-angle thrusts linked to the regional main detachment level in the Silurian shales of the Kirusillas Formation and an upper detachment level in the Los Monos Formation of Devonian age (Baby et al., 1992; Hernández et al., 2002; Fig. 2). Other minor detachment levels are developed in younger stratigraphic units like Ipaguazu Formation (Triassic age; Fig. 2; Dunn et al., 1995; Cruz et al., 2002; Hernández et al., 2002; Apreda et al., 2010). Some authors suggest deeper detachment levels within Ordovician units, or even older ones, which could have influenced some structures in southern sub-Andean (Moretti et al., 2002; Zapata et al., 2005; Hernández et al., 2018; Sánchez et al., 2020). As such, the proposal was made to involve an Ordovician wedge in the structured column working alongside the Silurian interval (Hernández et al., 2018; Sánchez et al., 2020). This Ordovician interval thickens toward the west from the western flank of the Charagua range. Thus, as the eastward movement through the basal sole fault takes place, a thicker Ordovician interval becomes involved in the deformation process, resulting not only in a higher structural position for the

anticlines but also for the back limb associated synclines. In line with this idea, each syncline reaches higher and higher structural positions to the west.

It is relevant to mention that, close to the southern end of the sub-Andean system as a thin-skinned thrust belt; the regional detachment surface dips toward the northwest due to load-driven subsidence combined with a tilting process caused by the Lomas de Olmedo rift basin opening during the Cretaceous period (Fig. 1; Starck et al., 2002).

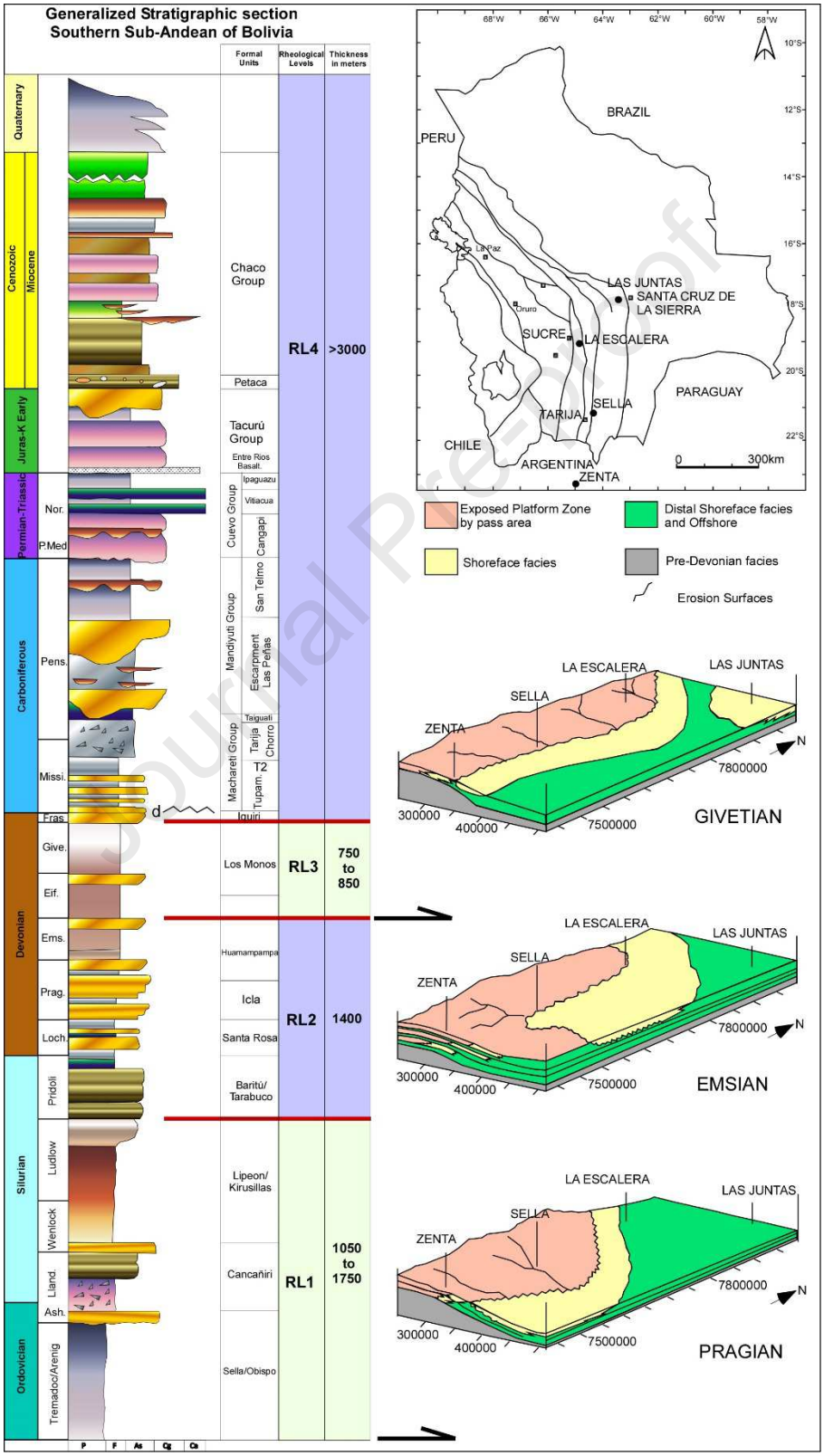

Fig. 2. Generalized stratigraphic section of southern sub-Andean of Bolivia (left). Devonian paleogeography in 3-D models showing variation of facies during Pragian, Emsian, and Givetian times (right) following Albariño et al. (2002). In the upper right corner, map of Bolivia showing the locations detailed in the 3-D models. RL = Rheological Levels (modified from Hernández et al 2018). Red lines show the limits between rheological levels representing changes in the mechanical behavior of the rocks involved in deformation. Black arrows show the main detachment levels.

The regional basal detachment surface (base of Rheological Level 1, after Hernández et al., 2018) used by different authors in their interpretation suggests a flat morphology with a constant westward gently dipping value of between 1.5 and 2.5 degrees, without showing angle changes. However, through a detailed analysis of the sedimentary infill (Fig. 3), Hernández et al. (2018) show the existence of pre-Andean basement reliefs related to extensional mechanisms that occurred since the Permian–Triassic, phenomena being enhanced during the Upper Triassic-Lower-Jurassic and/or Upper Jurassic-Lower Cretaceous, as well as erosive irregularities within the Carboniferous or the Devonian–Carboniferous boundary. These data suggest that a regular and continuous detachment level following a unique lithology, such as the ones involving the Ordovician or Silurian shales (Hernández et al., 2018; Sánchez et al., 2020), may not be the most realistic situation. In this way, an irregular detachment surface should be considered in regional balanced cross-sections construction involving the entire fold and thrust belt system, especially when integrated three-dimensional analysis is carried out. This would allow assessing the influence of these irregularities and heterogeneities on shortening transfer and topographic evolution. On the contrary, when a particular 2D-section-scale analysis involving a few structures is performed, a continuous and efficient detachment level could be considered.

The stratigraphic section involved in the fold and thrust belt deformation processes is formed by Ordovician to Cenozoic sedimentary, predominantly siliciclastic rocks, related to superimposed tectonically-driven basins, exceeding 6,500 meters thick (Fig. 2), synthesized as follows:

The Ordovician units are represented by siliciclastic marine successions, with significant shale thicknesses and prograding sandstones of a medium continuity, deposited in a foreland setting developed in a diachronic manner both from west to east and from north to south, (Erdtmann et al., 1995; Erdtmann, 1996; Erdtmann & Heuse, 1995; Erdtmann & Egenhoff, 1998; Heuse, Grahn & Erdtmann, 1999; Suárez Soruco & Díaz Martinez, 1996). Secondly, the Upper Ordovician to Lower Silurian interval, involving glacial deposits (Gagnier et al., 1996; Toro et al., 1992; Benedetto 1991; Suárez Soruco & Benedetto, 1996) and an active ocloyic phase tectonism, it is characterized during the Llandoverian interval in western Gondwana by extensional to transtensional phenomena with deposits spread in the Eastern Cordillera and Altiplano in Bolivia and the Chaco Basin in Paraguay (Grahn, 2005). The Wenlockian would represent a sag, with reduced deposits, in pelitic facies in Zapla (northwestern Argentina, Benedetto, 1991) or in carbonatic facies in Cochabamba (Bolivia, Sacta limestone, Merino Rodo, 1991; Cuatro Esquinas, Suárez Soruco & Benedetto, 1996). Thirdly, the Upper Silurian to Upper Devonian is characterized in Western Gondwana by the location of a backarc marine basin without deformation or an intracratonic basin, with the absence of relics of a magmatic arc (Álvarez et al., 2004; Albariño et al., 2002; Dalenz Farjat et al., 2002). In fourth place, within the Upper Devonian to Lower Carboniferous interval, the Frasnian greenhouse is followed by the latest Famennian to Tournaisian glaciation, widely documented in Bolivia (Suárez Soruco & Lobo Boneta, 1983; Perez Leyton, 1990; Wicander et al., 2011; Lakin et al., 2014) and in the rest of South America (Caputo et al., 2008; Streel et al., 2013; Rubinstein et al., 2017; Benedetto, 2018a), generating variable erosion levels and affecting the sedimentary record preserved below (Perez Leyton, 1990; Viera and Hernández, 2001; Wicander et al., 2011; Lakin

et al., 2014). The Upper Carboniferous to Lower Permian interval is represented by the completion of Pangea, structured during an icehouse that would have extended between the Upper Carboniferous and the late Lower Permian (Benedetto, 2018). The called Tarija basin would be considered as an intra-arc basin, with the same behavior as the Paraná basin, with a relatively low and uniform subsidence rate, little or no tectonic activity and lacking volcanism (Benedetto, 2018). In the Lower Permian, the climate becomes much more benign, producing carbonate rocks of the Copacabana Formation from Peru, from the Westphalian in northern Bolivia to the Lower Permian in central Bolivia (Grader et al., 2008; Dalenz Farjat & Merino Rodo, 1994; Merino Rodo & Blanco, 1990). Possibly, part of the aeolian deposits at the base of the Cuevo Group (Cangapi Formation) corresponds to the northern carbonate rock deposits. Ascending stratigraphically, the end of the Permian and the Triassic are the intervals where the Pangea Supercontinent suffers ruptures (Benedetto, 2018). In this time interval, most of the Andean and extra-Andean regions were subjected to extensional stresses that generated basins limited by faults in which continental and volcaniclastic sediments associated with acid and intermediate magmatism accumulated (Benedetto, 2018; Sempere et al., 2004). These first incipient distensive phenomena are the framework in which the Cuevo Group units develop in the southern sub-Andean region of Bolivia. The paleogeography of these rift basins would today be represented by the Eastern Cordillera, which would have been formed as an inversion of these narrow rifts developed between the Middle Permian and the Lower Cretaceous (Sempere et al., 2004). The Jurassic to Lower Cretaceous times in the South American continent, is characterized by extensional-type efforts dominated by the opening of the Atlantic Ocean. As a consequence, in the sub-Andean region of Bolivia, asymmetric grabens of N-NE orientation were developed and filled by aeolian and fluvial-lacustrine sedimentary rocks of the Tacurú Group with basaltic intercalations of different compositions (continental and alkaline tholeiitic rocks; Kusiak et al., 2014). Finally, the Cenozoic interval is related to the space and time evolution of the Andean fold and thrust belt.

The isopach maps developed by Hernandez et al., (2018) for time intervals separated by first order unconformities (Silurian to Miocene; Fig. 3), made it possible not only to identify changes and thickness variation trends in space but also to demarcate superimposed areas of higher or lower subsidence responding to basement controls. The location and magnitude of these structural peaks and troughs, as interpreted through thickness variation are, in several cases, concordant with planimetric irregularities in the anticline structures (inflection areas, plunges, and transfer zones). Based on this spatial relationship, a potential control of pre-Andean structures on shortening transfer may be inferred (Zubieta et al., 1996; Giraudo and Limachi, 2001).

Regional cross-sections developed by different authors have allowed determining shortening values in the southern sub-Andean, of up to 100 km in the northern part, close to the city of Villamontes (Dunn et al., 1995; Giraudo et al., 1999), whereas shortening values of around 60 km were calculated close to the Argentina–Bolivia international border (Mingramm et al., 1979; Baby et al., 1997; Kley and Monaldi, 1999; Hernández et al., 2002). Finally, the regional balanced cross-section developed by Sanchez et al., (2020) at the latitude of Cuevo River, a little south of the study area, presents a shortening value of 88 km (40%), involving the whole sub-Andean system, from the inter-Andean-sub-Andean limit to the west up to the Mandeyapecua structure to the east. This last value is shown in a consistent way with the shortening magnitudes determined in the present study considering that only the easternmost structures included in the regional section constructed by Sanchez et al., (2020) should be compared.

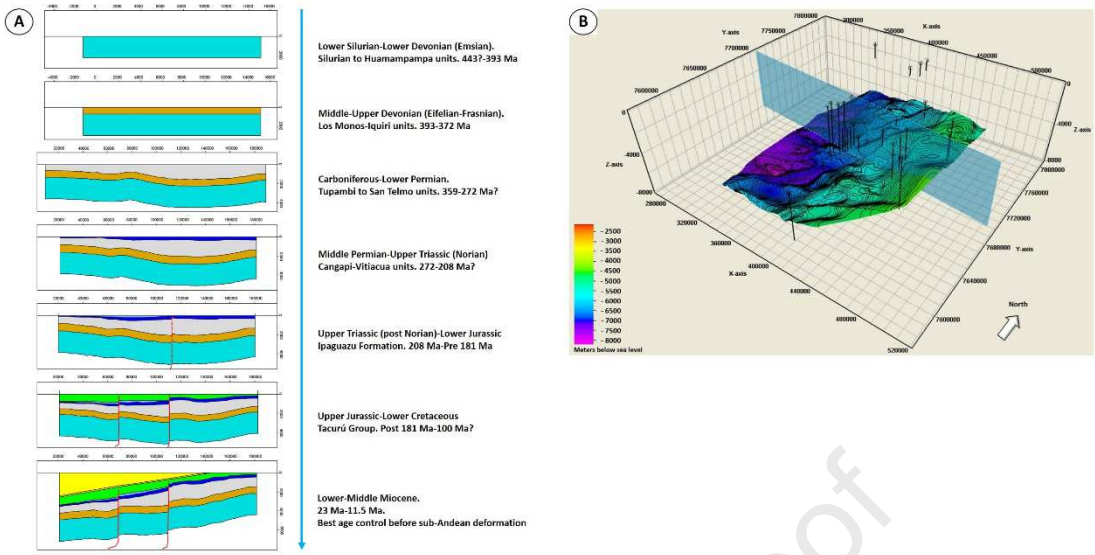

Fig. 3. A. Infilling stages for the main sedimentary cycles identified in the southern sub-Andean system. Location of the cross-section analyzed is displayed in Fig. 3B (light blue vertical rectangle). Polygon colors: dark green (Lower Silurian-Lower Devonian); brown (Middle–Upper Devonian); gray (Carboniferous–Lower Permian); blue (Middle Permian–Norian); light blue (Post Norian to pre-181 Ma Lower Jurassic); green (Upper Jurassic–Lower Cretaceous); orange (Oligocene-Lower Miocene); yellow (Miocene, 23–11.5 Ma). Red lines are interpreted faults. B. 3D structural surface for Ordovician top or Silurian base (location in Fig. 1B), leveled to 11.5 Ma timeline. Vertical black lines correspond to wells. Diagrams present 10 times vertical exaggeration (values in meters below sea level). Datum and coordinates: UTM, WGS84 (according to Hernandez et al., 2018).

Based on the location of the main detachment levels and the mechanical behavior of the stratigraphic units, the sedimentary column was divided, prior to Hernández et al., (2018), into three structural intervals (Mombrú and Aramayo Flores, 1986; Aramayo Flores, 1989; Baby et al., 1992; Starck et al., 2002; Leturmy et al., 2000; Giampaoli and Rojas Vera, 2018), assigning a parallel shear folding mechanism to the lower structural level strata. In their regional balanced cross-section, Hernández et al. (2002) evaluated the three-rheological-level structural outline, but trishear kinematic modeling (Erslev, 1991) was applied to the lower structural level. The algorithm related to this model is more characteristic of ductile inhomogeneous deformation. Finally, Hernández et al. (2018) proposed a structural framework based on the identification of four rheological levels (Fig. 2). Levels 1 and 3, with a shale-dominated composition (Ordovician to Kirusillas Formation and Los Monos Formation, respectively), are deformed as a weak isotropic material and can be simulated using Trishear kinematic modeling. On the other hand, rheological levels 2 and 4 (Tarabuco–Santa Rosa–Icla–Huamampampa Formations and Carboniferous–Cenozoic interval, respectively), with a sand/shale alternating composition, are structured as strongly heterogeneous intervals responding to the compressive stress field with parallel folding, as mentioned by Hardy and Finch, (2007). A simple shear kinematic model could be used to simulate this deformation. This behavior has been tested as a feasible model for the deep structure in significant oil/gas fields in Argentina and Bolivia (Hernández et al., 2011; Rocha and Cristallini, 2018). The four-rheological-level setting is the one considered suitable and applied in this publication for the structural analysis and chrono-kinematic modeling.

2.2. Sub-Andean fold-and-thrust belt evolution and time constraints

The sub-Andean fold-and-thrust system dynamics and its evolution over time, that is, the definition of fault-related anticlines timing, has been the subject of various studies both in its northern sector (Hernández et al, 2017; Constantini et al, 2018) as in its southern portion (Hernández et al., 2002; Echavarría et al., 2003; Anderson et al., 2018). Regarding this last sector and the study area of this work, the paleomagnetic, geochronological and thermochronological analyzes, suggest a fold-and-thrust belt developed from 9 Ma (Hernández et al., 2002; Echavarría et al., 2003) or ~ 11-8 Ma (Anderson et al., 2018) until today, as a result of an east-northeast-verging compressive stress field related to an eastward shortening transfer coming from the Eastern Cordillera and/or inter-Andean zone.

Timelines definition from the distal volcanic fall levels (tuffs) interspersed in the Miocene-Pliocene fluvial and marine deposits in the sub-Andean system have contributed to the understanding of the evolutionary dynamics of this fold-and-thrust belt. In this sense, geochronological analyzes have allowed the identification of space-and-time variations in sedimentation rates (Hernández et al., 2002; Echavarría et al., 2003), the definition of the growing ages of structures (Hernández et al., 2002), the age associated with marine transgressions (Hernández et al., 2005; Uba et al., 2007), sediment provenance analysis (Amidon et al., 2017), among other aspects.

The analysis and interpretation of paleomagnetic and thermochronological data within the sub-Andean zone included in the aforementioned contributions have resulted in different evolutionary scenarios aiming at fault-related folds with younger growing ages to the east (~ 9 to 2.5 Ma; Hernández et al., 2002) as well as their registered out-of-sequence fault movements (~ 5-4 to 0 Ma; Hernández et al., 2002) evidencing a “continuous” structural evolution with growing rates variation on the one hand, and a stop-and-go cyclical evolution model pointing to stagnation periods (~ 8.5 to 1.5 Ma) and advancing deformation intervals (from ~1.5 Ma on) as proposed by Anderson et al., (2018), on the other.

3. Methodology

The evolutionary analysis and the chronology of structures formation in compressive systems requires a multi-variable assessment regarding the mechanical-rheological stratigraphy of the rock column involved in the deformation, depth, inclination, morphology and connection between detachment levels, pressure of fluids and the presence of pre-existing structures or anisotropies among others. This analysis is achieved through the combination of subsurface data (2D-3D seismic and wells), surface data (structural mapping and stratigraphic surveys) and model-non-dependent analytical techniques such as geochronological (e.g. U-Pb in zircons) and thermochronological (e.g. fission-tracks and (U-Th-Sm)/He in apatites and zircons) determinations. This integrated-type analysis was carried out in the study area involving the structural transect developed in the southern sub-Andean system of Bolivia between the Incahuasi-Curuyuqui and Mandeyapecua structures as western and eastern extremes, respectively (Fig. 1).

The analysis performed in this work is based on the combination and integration of low-temperature thermochronological data (fission-tracks and (U-Th-Sm)/He, in apatites) and geochronological data (U-Pb SHRIMP in zircons), with geological constraints derived from surface and subsurface information. The aforementioned analytical techniques were applied to siliciclastic (sandstones) and volcanic (tuff levels) surface rock samples collected during field work (mapping and stratigraphic survey), in 2016-2017.

Apatite fission-track analyses were carried out in their entirety at the R&D Productive Technology Center, LA.TE. ANDES S.A. (Salta, Argentina). Concerning the apatite (U-Th-Sm)/He analyses, the tasks inherent to the preparation of samples, measurement of grains geometric parameters and their packing in Niobium tubes were developed at LA.TE. ANDES S.A., while the analytical measurements were developed in the Laboratory of Thermochronology of (U-Th-Sm)/He in the city of Prague (Czech Republic) in the case of the structures of Curuyuqui-Pirirenda, Carohuaicho and Tatarenda, and at the Jackson School of Geosciences in Austin, Texas (USA) for the Borebigua, Charagua and Mandeyapecua structures. Finally, regarding the U-Pb analyses, the procedures inherent to sample preparation, selection of crystals to be mounted and the definition of measurement spots by means of cathodoluminescence and back-scattering images were developed at LA.TE. ANDES S.A., while the corresponding isotopic measurements, data reduction, and age calculation were carried out at the Geosciences Institute of the University of São Paulo (SHRIMP IIe, Brazil).

3.1. Geochronology. Zircon U-Pb dating

U-Th/ Pb technique is based on the physical principle of radioactive decay of Uranium (^{238}U and ^{235}U) and Thorium (^{232}Th) into stable daughter isotopes of Lead (^{206}Pb, ^{207}Pb and ^{208}Pb, respectively) through chains completely independent decay cells involving numerous intermediate isotopes.

The stability of the U-Th/ Pb system derives from the fact that the volume diffusion of Pb through minerals network is generally slow compared to other thermochronological techniques, such as those based on the diffusion of He or the closure of fission tracks, which allows to know the formation ages of minerals or rocks. U–Th–Pb isotopic system in zircon will typically have a closure temperature greater than 900 °C (Cherniak and Watson, 2001; Lee, 1997).

U/Pb measurements were carried out on selected zircons from tuff samples in the study area through SHRIMP II (Sensitive High Resolution Ion Micro Probe) equipment. This technique allows for point isotopic analysis (~ 20 μm x 3 μm) on individual zircon grains, avoiding inclusions or fractures as much as possible. Measurements include core and edge of grain in some cases, generally, only one spot per analyzed zircon was measured, reaching between 15 to 37 measurement spots per sample (Tab. S1). The results were finally processed using the SQUIZ program (Ludwig, 2008) and the ISOPLOT/Ex program (version 3.00; Ludwig, 2003).

The combination of these measurements with the low-temperature thermochronological data set obtained in this study has contributed significantly to the definition of t-T coordinates in the corresponding numerical modeling. In this sense, the timelines definition based on U-Pb measurements applied on Miocene tuff levels permitted analyzing the most recent history of the sub-Andean fold and thrust system.

3.2. Thermochronology

Thermochronology is based on the accumulation and thermally controlled retention of isotopic daughter products and linear crystal defects produced during the radioactive decay of parent. Due to the temperature sensitivity of the thermochronometers, the ages provide information about the cooling history of the rock, rather than mineral crystallization ages (although in some cases they do record crystallization ages as well).
For this research, apatite fission-track (AFT), and apatite (U-Th-Sm)/He dating (AHe) were performed on Devonian to Miocene sedimentary and volcanic rocks involving several fault-

related anticlines in the study area (Fig. 1). Whenever possible the two thermochronometry dating techniques were applied to the samples, allowing a more robust evaluation of the spatial and temporal cooling of the sampled rocks. Thirty-six samples contained apatite grains in quantities, to allow AFT and AHe dating (Figs. 1, S1-S2-; Tabs. S2-S3).

3.2.1. Apatite fission-track (AFT) thermochronology

Fission track thermochronology is based on the retention of radiation damage (fission tracks) formed during the spontaneous fission of ^{238}U in uranium-bearing minerals (commonly apatite or zircon). The closure temperature, that is the temperature of the dated mineral when the system closes and daughter start to accumulate while rock is undergoing steady monotonic cooling (Dodson, 1973), is on the order of 110 °C (±10 °C)/10Myrs for the AFT system, although it depends on apatite composition and cooling rate (e.g., Gleadow and Duddy, 1981; Gleadow et al., 1986; Green et al., 1989). On the other hand, fission tracks orientation in relationship with the crystallographic c-axis is to be considered within the annealing conditions (Green et al., 1986; Ketcham et al., 1999, 2007). The partial annealing zone (PAZ, Gleadow and Fitzgerald, 1987) for apatite is from ~120 °C/10Myrs to 60 °C/10Myrs (e.g., Reiners and Brandon, 2006). Determining the concentration of ^{238}U and density of spontaneous fission tracks allows the determination of fission-track ages that, together with the kinetic parameter of confined track lengths, may provide constraints on the thermal history of rocks as they traverse the upper 4–5 km of the crust.

Apatites compositional variations (F, Cl, OH, REE) affect the annealing behavior of fission tracks (e.g. Green et al., 1986). Several kinetics parameters were used to understand this, as Dpar, Cl content (apfu or %), r_{mr0}. The most commonly used is Dpar (e.g. Ketcham 2016, Donelick et al., 2005). DPar is the etch pit diameter parallel to the c-axis, specified in microns, and is positively correlated with thermal resistance. The apatites with Dpar < 1.75 are less resistant to thermal annealing than apatites with higher Dpar (Donelick et al., 2005). For this work, Dpar was the kinetic parameter chosen to model.

The samples included in the present study were irradiated in Reactor RA-3 (Ezeiza Atomic Center, Buenos Aires). Measurements were made using a Zeiss® AXIO Imager Z2m binocular microscope with advanced research phototube, with Autoscan® equipment and associated software. The entire system is controlled by TrackWorks® Autoscan® Software with which the tracks density counting and measurement of kinetic parameters (confined-track lengths and DPar© values) were performed, to carry out the corresponding numerical modeling (HeFTy®, Ketcham, 2005; Ketcham et al., 2007a, b; 2009). Fission-track ages were determined using the ζ-value method (external detector method, EDM) described by Gleadow (1981), Hurford and Green (1982, 1983) and Wagner and Van den Haute (1992). A minimum of 19 grains per sample was counted (Tab. S2). Data processing was performed using the TrackKey© program (Dunkl, 2002) for calculating ages and their associated error (1σ). In those samples with high dispersion in the age distribution by grain (χ2-test with values <5% with respect to 1σ-error, Galbraith, 1981), the population analysis was performed using the BinomFit© Software (Brandon, 1992, 1996, 2002).

3.2.2. Apatite (U-Th-Sm)/He (AHe) thermochronology

The (U-Th-Sm)/He thermochronology is based on the accumulation of ^{4}He during the α-disintegration of ^{238}U, ^{235}U, ^{232}Th, their daughter products and ^{147}Sm. The closure temperature (Tc) of mineral grains is dependent on: activation energy (E), a geometric factor for the crystal form (A), thermal diffusivity (D_0), the length of the average diffusion pathway from the interior

to the surface of the grain (a) and the cooling rate at closure temperature (dT/dt) (Dodson, 1973). In general, the Tc of the apatite (U-Th-Sm)/He system is ~70°C/1 Myr for cooling rates of 10°C/Myr, subgrain domain sizes > 60 µm and an activation energy of about 36 kcal/mol, and a log(D_0) of 7.7±0.6 cm²/s (Farley 2000). The Partial Retention Zone (PRZ) for the (U-Th-Sm)/He system in apatites is defined between 70 °C/1 Myr and 40 °C/1 Myr (Wolf et al., 1996; Farley, 1996, 2000, 2002; Stockli et al., 2000). Different calibration models have been proposed for the (U-Th-Sm)/He system in apatites (Wolf et al., 1996; Farley 2000; Shuster et al., 2006; Flowers et al., 2009) in relationship with the role of crystal size on effective diffusion, stopping distances, gain or loss of radiogenic He generated within an outer rim of the mineral grain, and the correction for radiation damage on He diffusion.

(U–Th–Sm)/He analysis was performed on suitable single grains of apatite. The grains were selected, and size measured. Since the He analytical technique requires well-defined crystals without any cracks, mineral or fluid inclusions, the apatite mineral concentrates were screened for appropriate grains. Three to six grains per sample were selected and send for analytical work (Tab. S3). The radiogenic ^{4}He was extracted in an ultrahigh vacuum chamber through heating with an Nd-YAG laser. The released gas was subsequently measured and quantified with a Balzers Prisma QMS-200 quadrupole mass spectrometer. The grains were recovered, digested and spiked with known amounts of tracer-isotopes (^{230}Th-^{235}U-^{147}Sm). In order to minimize effects caused by undetected mineral inclusions, apatite grains were bombed to ensure complete digestions as described in Vermeesch et al. (2007). Thereafter, U-Th content of the dissolved crystals was measured on a Fisons/VG PlasmaQuad II ICP-MS. Further analytical details are documented by Biswas et al. (2007), Stockli et al. (2003) and Wipf (2006).

Apatite (U-Th-Sm)/He ages obtained in the present study were combined with the apatite fission-track data for the development of the corresponding numerical modeling, contributing to the chrono-kinematic interpretation of the structures involved in the study area and the corresponding quantitative analyzes.

3.3. Thermal modeling: time-Temperature (t-T) paths and geological model

Thermal modeling of thermochronological data allows us to reconstruct the heating and cooling history for crustal segments or specific structures like fault-related folds. HeFTy® (v.1.9.3.74) (Ketcham, 2005; Ketcham et al., 2007a, b; 2009) was used to test time-Temperature (t-T) paths against the thermochronological data set. The software code runs paths through t-T-constraints to find possible solutions for a t-T-history considering the input data.

Thermal modeling was performed considering the following selection parameters for the samples in the study area:

1) General:

- Structural location of the sample.
- Stratigraphic location of the sample.
- Possibility of combining thermochronometers for joint modeling.

2) Thermochronological data:

Apatite fission-track system (AFT):

- Amount of grains measured. Single grain ages.

- Amount of confined spontaneous fission-track lengths measured (corrected for c-axis related angle (Donelick et al., 1999; Ketcham, 2017, 5.5M, 2009)), etch pit size (Dpar®), annealing kinetics of Ketcham et al. (2007a, b).

- AFT Central ages vs Stratigraphic ages.

- Single grain ages distribution and populations identified through statistics (binomial peak adjustment method performed using the BinomFit© Software, Brandon, 1992, 1996, 2002).

Apatite (U-Th-Sm)/He system (AHe):

- U-, Th-, Sm-, and He concentration.

- Radius of the single grains and uncorrected single grain ages. Ft value (α-correction) > 0.5.

- eU (effective Uranium value) given by eU= [U] + [0,253*Th] + [0,0053*Sm]

- Diffusion kinetics of Flowers et al. (2007, 2009), Wolf et al., (1996), Farley (2000) or Shuster et al., (2006), depending on the case. It must be stated that, in principle, the RDAAM kinetic model by Flowers et al., (2009) was considered as the most suitable and updated model taking into account the influence of radiation damage on Helium diffusion within apatite grains. In some cases, it was not feasible to apply the model mentioned, thus, alternative kinetic models were tested considering the influence of crystal size on effective diffusion, stopping distances, gain or loss of radiogenic He generated within an outer rim of the mineral grain, and particular chemical composition of apatite grains (Wolf et al., 1996; Farley, 2000 or Shuster et al., 2006).

To define a possible t-T-evolution we tested our thermochronological data against a geological evolution model and an inverse, numerical model was performed (Fig. 4, Fig. S3). The geological evolution model is determined by t-T-constraints and based on published knowledge of the geological history (Hernández et al., 2002; Echavarría et al., 2003; Hernández et al., 2005; Uba et al., 2007; Amidon et al., 2017; Anderson et al., 2018; Hernández et al., 2018. Figs. 2-3). Therefore, specific t-T-constraints (Tab. 1, Tab. S4) were set corresponding to 2016-2017 field data (mapping and stratigraphic survey). In this way, particular structural and stratigraphic constraints were applied to each sample modeled in relationship with geographic and geological location, timelines available, magnitude and distribution of thickness values per time interval. On the other hand, a homogenous paleo-geothermal gradient of 30 °C/km was applied to the entire modeled time (starting point for thickness-to-temperature conversion), giving the possibility of higher and lower values during numerical modeling constraints definition. Finally, paleo-surface temperatures for Devonian, Carboniferous and Permian-Mesozoic-Cenozoic time intervals was assumed as 20 ± 5 °C, 10 ± 5 °C and 20 ± 5 °C in correspondence with paleolatitude values for the study area (Wygrala, 1989; Scotese et al., 1992,1999).

Table 1. Numerical modeling constraints. Thickness per time interval column represent the magnitude of each stratigraphic interval being deposited (first order unconformities separating) or estimated thickness being eroded (numbers in parentheses), integrating both the regional and local scale. (1) Growth strata thickness dependent on structural position. (2) Structural timing related to thermochronological data (apatite (U-Th-Sm)/He). Supporting information in Tab S4.

Constraint	Geological Event description	Time (Ma)	Thickness per time interval (m)
10	Structural Timing[2]	7.1-0	(250-1600)
9	Yecua Fm. - Chaco Group (growth strata included)[1]	8-0	785-3060
8	Petaca Fm.	34-23	10-130
7	Tacurú Group (partial absence)	140-34	(500-900)
6	Tacurú Group (accumulation)	163-100	750-1550
5	Cuevo Group (Cangapi+ Vitiacua Fms.) (absence)	208-181	(150-585)
4	Cuevo Group (Cangapi+ Vitiacua Fms.) (accumulation)	272-208	150-585
3	Mandiyutí Group	323-299	218-1178
2	Macharetí Group	359-323	495-930
1	Iquiri-Saipurú Fms.	383-359	0-250

Constraints definition integrates both regional and local observations concerning thicknesses preserved per time interval and thickness not preserved or estimated to have been eroded (Tab. 1). The Upper Devonian, Lower Carboniferous, Upper Carboniferous, Upper Jurassic to Lower Cretaceous, Oligocene to Lower Miocene and Upper Miocene to date units were deposited, identified and measured in the study area through mapping and stratigraphic survey. The Permian to Triassic units were identified and measured regionally in the southern sub-Andean system, but not preserved within the study area as neither does the Upper Carboniferous San Telmo Formation. The stratigraphic age and regional thickness distribution for each stratigraphic interval supporting the geological constraints defined have their origin in:

1. Iquiri-Saipurú Fms. Sedimentation. Upper Devonian units based on Perez Leyton, (1990), Albariño et al., (2002), Dalenz Farjat et al., (2002), Álvarez et al., (2004), Troth et al., (2011), Hernández et al., (2018).

2. Macharetí Group. Sedimentation. Lower Carboniferous units based on Suárez Soruco and Lobo Boneta, (1983), Perez Leyton, (1990), Caputo et al., (2008), Wicander et al., (2011), Streel et al., (2013), Lakin et al., (2014), Rubinstein et al., (2017), Benedetto, (2018a), Hernández et al., (2018).

3. Mandiyutí Group Sedimentation. Upper Carboniferous units based on Viera and Hernández, (2001); Benedetto, (2018); Hernández et al., (2018).

4. Cuevo Group (Cangapi+ Vitiacua Fms.) (Accumulation) and 5. Cuevo Group (Cangapi+ Vitiacua Fms.) (Absence). Permian to Triassic units based on Beltan et al., (1987), Suarez Riglos and Dalenz Farjat, (1993), Hernández et al., (2018), Gallo et al., (2019).

6. Tacurú Group (Accumulation) and 7. Tacurú Group (partial Absence). Upper Jurassic to Lower Cretaceous units based on Suárez Riglos and Souza Carvalho, (2018), Kusiak et al., (2014), Hernández et al., (2018).

8. Petaca Fm. Sedimentation. Oligocene to Lower Miocene units based on Marshall and Sempere, (1991), Erikson, (1998), Hernández et al., (2018).

9. Yecua Fm. - Chaco Group (growth strata included). Sedimentation. Upper Miocene to date units based on Erikson, (1998), Hernández et al., (2002), Hernández et al., (2005), Uba et al., (2007, 2009), Hernández et al., (2018), Sánchez et al., (2020), and U-Pb ages on zircons included within the present publication.

10. Structural Timing. Upper Miocene to Pliocene-Pleistocene cooling ages based on apatite (U-Th-Sm)/He measurements presented in this study and published data (Anderson et al., 2018).

The interpretation of the study area in relationship with heating and cooling events, and the estimation of exhumation and subsidence rates, were performed based on the “weighted-mean”

paths of the modeled t-T evolution, summarizing all possible t-T paths. The cooling and heating rates (constant slope segments within t-T trajectories) were divided by a fixed geothermal gradient (30°/km) to obtain an exhumation and subsidence rate, respectively. All rates are expressed as positive rates, and relate to exhumation or subsidence according to the decrease and increase of temperature over time. On the other hand, the corresponding uncertainty derived from numerical modeling is statistically expressed through the goodness of fit (G.O.F) values of 50% and 5%, represented by Good or Acceptable t-T paths, respectively.

The application of multiple thermochronometers and the included geological constraints allowed the development of the corresponding numerical models for the definition of t-T trajectories (HeFTy® software; Ketcham, 2005), making it possible to identify and characterize heating-cooling events that have occurred since the deposition of the stratigraphic units analyzed to date, providing important definitions to the oil and gas system.

3.4. Structural analysis: chrono-kinematic modeling

The structural analysis was developed through the construction and restoration of balanced sections in the Andino 3D® software using structural and stratigraphic surface data, and subsurface data corresponding to well information (tops, logs, dipmeters) and 2D seismic (Fig. 5, Fig. S4). The developed cross-sections were integrated three-dimensionally, providing coherence and solidity to the corresponding interpretation. On the other hand, the incorporation of the data emerging from the analytical techniques described allowed the development of a chrono-kinematic analysis of the deformation (Fig. 8), enabling to characterize the chronology of growth of the structures and their space-and-time link, the quantitative analysis of exhumation rates, the transfer of shortening between structures, etc. This type of analysis requires a sampling design in transects arranged transverse to the structural features in the area of interest, making it possible to take rock samples from all the outcropping stratigraphic units both in the nuclei and in the front-limbs and back-limbs of successive or adjacent anticlines and synclines (Hernández et al., 2018; Hernández et al., 2020). The integral sampling of the analyzed structures will allow a complete chrono-kinematic reconstruction from the definition of t-T trajectories, while a sampling limited, for example, to the core of the anticline structures (older stratigraphic units), will only allow characterizing their most recent history.

3.5. Oil and Gas system numerical modeling

The integration of geological and thermochronological data led to the development of the Oil and Gas system modeling presented in the study area. A 1D Petromod® model was constructed for the syncline located between Charagua and Borebigua structures (Fig. 9, Figs. S5-S7, see location in Fig. 1C) for assessing and characterizing the hydrocarbon perspectives within the area. The modeling performed integrates the input data related to geological history, sedimentation age, thicknesses (preserved and eroded), lithological composition, characterization of petroleum system elements (source rock, seal rock, reservoir rock, overburden rock and trap timing), and kinetic and geochemical parameters (Total Organic Content-TOC, Hydrogen Index-HI) (Fig. S5), the latter based on published information (Cruz et al., 2002, 2008).

The modeling achieved permitted evaluating the possible source rocks in the area as described by Cruz et al., (2002, 2008): a) Emsian-Eifelian-Givetian interval (Los Monos Formation), b) Lochkovian interval (fine-grain sediments within the Santa Rosa Formation) and c) Silurian interval (Kirusillas Formation) (see stratigraphic location in Fig. 2).

To complete the thermal maturity data (modeled Vitrinite Reflectance values; %Ro, Fig. S7), an assessment of the thermochronological data set in Charagua was made, combining AFT-AHe data and the t-T numerical modeling developed for the Upper Devonian unit (Iquiri Formation, Charagua structure). In this way, it was possible to obtain a burial curve for the thermal history model developed, following and being calibrated with the weighted-mean path obtained with HeFTy® numerical modeling.

4. Results

Geochronological and Thermochronological data

The field tasks corresponding to the structural mapping and the stratigraphic survey carried out between 2016 and 2017, allowed the collection of clastic and volcanic samples on which the low-temperature thermochronology analyzes (fission-tracks and (U-Th-Sm)/He, on apatites) and geochronological studies (absolute dating, U-Pb SHRIMP on zircons) were performed. In this sense, a total of 56 samples corresponding to Devonian, Carboniferous, Mesozoic (Jurassic-Cretaceous) and Cenozoic (Oligocene-Miocene) units were collected, from which the samples were selected for the application of the aforementioned analytical methods (Fig. 1, Fig. S1; Tabs. 2-5, Tabs. S1-S3).

The results obtained from the thermochronometers analyzed (apatite fission-track, apatite (U-Th-Sm)/He and zircon U-Pb SHRIMP) and the numerical models performed allowed to reconstruct the complete t-T evolution of the units analyzed from the deposition age up to the present, allowing the definition and characterization of heating and cooling events, interpreted as subsidence-burial and exhumation-structural growth phenomena, respectively.

4.1. Zircon U-Pb SHRIMP (Sensitive High Resolution Ion Micro Probe) data

In the particular case of the structural transect developed between the structures of Curuyuqui and Mandeyapecua, the determination of ages by U-Pb SHRIMP in zircons corresponding to 5 tuff levels have allowed to accurately define the age of the Miocene deposits present in the area (Fig. 1; Tab. 2, Tab. S1). U-Pb ages were calculated based on the youngest age-cluster within the samples. These ages are interpreted as sedimentation ages, while older grains included within the samples are associated to detrital components and were not included in the Miocene age cluster calculation (Tab. 2, Tab. S1).

Table 2. Zircon U-Pb SHRIMP data of tuff layers in the study area (interpreted sedimentation age). See supporting U-Pb data in Tab. S1. n: number of analyses from the total # included in the calculated weighted mean date. MSWD: mean square of weighted deviates. WGS84 datum used for coordinates.

			Coordinates				
Sample	Structure	Stratigraphic Unit	Latitude (°S)	Longitude (°W)	U-Pb age (Ma)	n	#
A-039	Charagua	Chaco Gp.	-19.3532	-63.1311	6.82 ± 0.29 (MSWD=1.9)	11	27
A-045	Mandeyapecua	Chaco Gp.	-19.3633	-63.0809	6.98 ± 0.31 (MSWD=5.5)	10	19
A-051	Borebigua	Chaco Gp.	-19.3710	-63.2307	8.57 ± 0.78 (MSWD=0.04)	6	36
A-167	Curuyuqui	Chaco Gp.	-19.4544	-63.3416	8.86 ± 0.21 (MSWD=0.09)	9	14
A-171	Tatarenda	Chaco Gp.	-19.1913	-63.2622	9.01 ± 0.21 (MSWD=0.28)	15	15

Zircon U-Pb SHRIMP analyzes developed in 5 samples corresponding to volcanic levels located, from west to east, in the Pirirenda syncline, Itai syncline, western flank of Borebigua structure, eastern flank of Charagua anticline and Mandeyapecua structure, determined the ages 8.86 ± 0.21 Ma (A-167), 9.01 ± 0.21 Ma (A-171), 8.57 ± 0.78 Ma (A-051), 6.82 ± 0.29 Ma (A-

039) and 6.98 ± 0.31Ma (A-045), respectively (Tab. 2, Tab. S1). This constitutes a relevant aspect of evaluating the space-and-time variation of the Miocene deposits as the lithostatic column above the underlying units sampled with thermochronological objectives, allowing to characterize the Miocene-Pliocene subsidence processes.

4.2. Apatite fission-track data

Apatite fission-track analysis (AFT) were carried out on 11, Devonian and Carboniferous siliciclastic sedimentary rock samples, distributed in the structures of Carohuaicho, Borebigua and Charagua (Figs. 1, 5, Figs. S1, S2; Tabs. 3-4, Tab. S2).

Apatite fission-track analysis lead to central ages between 57.6 ± 6.5 Ma and 359.6 ± 32.2 Ma (Tab. 3, Tab. S2). The apatite fission-track ages obtained for the samples in the study area are younger than the corresponding stratigraphic ages, with the exception of a sample from the Upper Carboniferous of the Charagua structure (A-044, Central Age AFT: 359.6 ± 32.2 Ma). The statistical population analysis using all single grain ages, allowed the identification of samples with multiple age populations and samples with homogeneous age distributions or single populations (Tab. 3, Fig. S2). In this sense, the recurrence of ages between 138.4 ± 14.7 Ma and 166.8 ± 12.9 Ma must be mentioned in the eastern sector of the study area (structures of Borebigua and Charagua), determined from a Devonian sample with unimodal single grain age distribution (A-054: 138.4 ± 14.7 Ma, $P(\chi)^2 = 15.02$) as per Devonian and Lower Carboniferous samples with calculated single grain age populations with wide predominance of these ages (79.8 to 81.7% of the grains measured; A-042: 165.1 ± 13.35 Ma; A-043: 149.4 ± 13.2 Ma; and A-101: 166.8 ± 12.9 Ma). Finally, the measurement of confined-track lengths and Dpar® values, in addition to the individual ages mentioned (Tab. 4, Tab. S2), allowed conferring solidity to the development of the numerical modeling of the samples in the study area.

Table. 3. Apatite Fission Track Data in the study area. AFT central ages calculated using IRMM 540 and z-IRMM 540 dosimetric glasses between 300-400. ρs: density of spontaneous fission-tracks (x 105 tracks/cm2) measured in apatite grains; Ns: total number of spontaneous fission-tracks; ρi and ρd: density of fission-tracks induced in the samples and in the dosimetric glasses respectively (x 105 tracks/cm2) in the external detector (g = 0.5); Ni: total number of induced fission-tracks in the sample; P (χ2): probability of obtaining a value of χ2 for n degrees of freedom (where n = number of crystals -1); a probability> 5% is indicative of a homogeneous population. Samples with probability <5% must be analyzed with the binomial peak adjustment method. P1, P2 and P3 are the averages of the different populations statistically calculated using the Binomfit© software (numbers in parentheses indicating the percentage of grains included in each population). See supporting AFT data in Tab. S2 and Fig. S2. WGS84 datum used for coordinates.

				Coordinates			Dosimeter		Sp. fission-tracks		In. fission-tracks						
Sample	Structure	Stratigraphic unit	Formation age (Ma)	Latitude (°S)	Longitude (°W)	U (ppm)	ρD	n	ρ_s	N_s	ρ_i	N_i	P(χ)2	AFT central age (Ma) ± 1s	P1 ± 1s (%)	P2 ± 1s (%)	P3 ± 1s (%)
A-042	Charagua	Iquiri Fm.	383-372	-19.3524	-63.1547	31.3	6.575	33	19.759	1,401	14.597	1,035	0.1	148.9 ± 13.1	96.6 ± 15.05 (20.2)	165.1 ± 13.35 (79.8)	
A-043	Charagua	Iquiri Fm.	383-372	-19.3534	-63.1530	26.6	6.657	19	15.700	818	10.900	571	0.97	163.4 ± 16.8	149.4 ± 13.2 (81.7)	289.3 ± 77.6 (18.3)	
A-044	Charagua	Taiguati Fm.	330-315	-19.3519	-63.1460	19.4	6.680	23	30.910	1,940	9.060	569	26.88	359.6 ± 32.2	-	-	-
A-052	Borebigua	Chorro Fm.	359-323	-19.3908	-63.1924	24.8	6.822	30	18.620	1,331	9.364	669	0.02	216.4 ± 21.4	195.3 ± 20.1 (59.6)	298.7 ± 37 (40.4)	
A-054	Borebigua	Iquiri Fm.	383-372	-19.3721	-63.1916	25.0	6.690	24	15.530	455	11.844	347	15.02	138.4 ± 14.7	-	-	-
A-101	Borebigua	Tupambi Fm.	359-331	-19.4530	-63.1807	45.1	6.700	24	29.320	2,087	22.100	1,578	0	134.1 ± 18.2	58.9 ± 6.9 (19.5)	166.8 ± 12.9 (80.5)	
A-159	Borebigua	Escarpment Fm.	323-299	-19.3533	-63.2046	22.7	11.980	26	13.700	730	16.800	892	0	162.6 ± 20.6	86.8 ± 13 (34.8)	218.5 ± 22.9 (65.2)	
A-160	Carohuaicho	Iquiri Fm.	383-372	-19.1302	-63.3444	25.6	11.530	39	6.100	367	20.900	1,264	0	57.6 ± 6.5	35.8 ± 4.7 (53.1)	91.3 ± 10.8 (46.9)	
A-161	Carohuaicho	Tupambi Fm.	359-331	-19.1310	-63.3456	23.4	11.420	34	21.900	3,356	17.900	2,743	0	241.9 ± 18.9	194.5 ± 17.4 (31.3)	251.5 ± 23.5 (50.6)	330.7 ± 46.9 (18.1)
A-197	Carohuaicho	Escarpment Fm.	323-299	-19.3004	-63.3207	22.1	11.070	28	23.800	2,619	16.250	1,781	0	293.2 ± 30.6	134 ± 14.7 (11.1)	278.4 ± 20.4 (69.6)	565.6 ± 69.7 (19.3)
A-200	Carohuaicho	Escarpment Fm.	323-299	-19.1722	-63.3447	16.9	10.960	35	20.400	1,864	12.700	1,162	0.01	296.8 ± 26.7	246.3 ± 22 (59.1)	398.9 ± 43.2 (40.9)	

Table. 4. Apatite fission-track lengths and Dpar data. n CT: number of confined track lengths measured; CT mean: Average of confined track lengths measured; CT std: standard deviation of the confined track lengths per sample; CT skew: kurtosis of the distribution relative to the average value (measure of the asymmetry of the distribution); CT-c mean: an average of confined track lengths corrected by c-axis; n Dpar: number of measured etch pit dimensions; Dpar mean: average DPar per sample. See supporting data in Tab. S2.

Sample	n CT	CT mean (µm)	CT std (µm)	CT skew	CT-c mean (µm)	CT-c std (µm)	CT-c skew	n Dpar	Dpar mean (µm)	Dpar std (µm)	Dpar skew
A042	22	9.6	1.1	-0.3	14.6	0.8	0.5	153	1.3	0.2	1.3
A043	24	10.0	1.3	-0.7	12.4	0.7	-0.7	200	1.2	0.2	1.4
A044	63	10.0	1.5	-0.1	12.5	0.9	1.2	105	1.5	0.2	0.6
A052	32	10.5	1.3	0.2	15.7	0.8	0.6	148	1.3	0.2	0.3
A054	22	8.9	1.7	4.8	11.7	1.1	5.1	94	1.5	0.1	-0.4
A101	46	9.2	1.3	0.2	14.2	0.6	0.0	100	1.6	0.2	5.6
A159	21	10.3	2.3	3.2	12.3	1.1	0.1	101	1.5	0.2	3.4
A160	5	9.7	1.1	-2.6	12.1	0.7	-1.6	156	1.5	0.1	1.7
A161	112	9.9	1.8	1.7	12.5	0.7	-0.5	172	1.6	0.2	0.4
A197	73	10.9	1.3	-0.5	13.0	0.8	-0.1	137	1.4	0.1	0.0
A200	57	11.4	1.4	-0.4	13.3	0.8	-0.8	173	1.6	0.2	2.1

Apatite fission-track length and etch pit size (Dpar®) data was acquired on the 11 samples. In average, 5.1 Dpar®/grain, and 139.9 Dpar®/sample, respectively were measured, meaning a total of 1539 etch pit sizes for all apatite grains (Tab. 4; Tab. S2). The mean Dpar® value for each sample ranges between 1.2 and 1.6 μm with an average Dpar® value of 1.4 μm. This relatively narrow range possibly indicates a homogeneous composition concerning the fluorine and chlorine content of apatite. Moreover, the use of the parameter R_{mr0} was also considered, calculating said parameter from the measurement of DPar according to the publications of Ketcham (1999, 2007) (Tab. S2), and in no case was it observed compositional variation with respect to ages. Both the DPar and R_{mr0} values show overlap in the composition between the grains. In all cases, the values obtained for R_{mr0}, exceeded the value of R_{mr0}> 0.80 and DPar <1.75, which would indicate fluorapatites, with a low resistance to annealing. Finally, we measured 43.4 track lengths per sample (maximum of 112), meaning 477 track lengths of confined fission-tracks for all samples (Tab. 4). Mean track lengths vary between 8.9 μm and 11.4 μm. The correction of the confined track lengths for their crystallographic orientation led to values between 11.7 μm and 15.7 μm (Ketcham et al., 2007, HeFTy®, v.1.9.3.74).

4.3. Apatite (U-Th-Sm)/He data

36 sedimentary rocks samples and volcanic tuff samples (Devonian, Carboniferous, Jurassic-Cretaceous, Oligocene, Miocene) distributed, from west to east, in the structures of Curuyuqui-Pirirenda, Carohuaicho, Tatarenda, Borebigua, Charagua and Mandeyapecua, were analyzed using the apatite (U-Th-Sm)/He technique (Fig. 1, Fig. S1; Tab. 5, Tab. S3).

The 36 samples exhibited variable individual α-ejection corrected AHe ages (Ketcham et al., 2011) with high frequency in the Miocene-Pliocene-Pleistocene interval, ages between 15.9 ± 1.0 Ma and 1.2 ± 0.01 Ma, with mean AHe ages between 8.8 ± 2.2 Ma and 2.0 ± 0.2 Ma (Tab. 5, Tab. S3). The individual ages measured are in relation to the stratigraphic age of the samples, generally increasing the dispersion and variability of AHe ages towards the younger clastic samples stratigraphically speaking. The Devonian samples have very young AHe ages limited between 5.3 ± 0.3 Ma and 2.0 ± 0.1 Ma (except for two grains belonging to samples A-042 and A-160), reflecting cooling under the reference temperature defined for the apatite (U-Th-Sm)/He system and allowing, in this case, to characterize the most recent thermal events in the study area. Samples from the Lower Carboniferous show slightly older AHe ages between 7.3 ± 0.4 Ma and 3.2 ± 0.2 Ma, exhibiting few older ages outside this range (Tab. S3). On the other hand, the samples belonging to the Upper Carboniferous present individual AHe ages varying between 215.7 ± 9.0 Ma and 2.3 ± 0.1 Ma. The results obtained for the Upper Carboniferous samples in the study area depend on their structural position and the Miocene-Pliocene-to-date subsidence-burial history.

Table. 5. Apatite (U-Th-Sm)/He data in the study area. See supporting (U-Th-Sm)/He data in Tab. S3. n (a,m): number of grains analyzed, grains used in mean age. WGS84 datum used for coordinates.

				Coordinates				
Sample	Structure	Stratigraphic Unit	Formation age (Ma)	Latitude (°S)	Longitude (°W)	Mean age (Ma)	Error (2s)	n (a,m)
A-034	Mandeyapecua	Chaco Gp.	< 6.98	-19.3624	-63.0838	62.6	40.7	(3,3)
A-035	Charagua	Ichoa Fm. (Tacuru Gp.)	163-100	-19.3520	-63.1412	241.0	98.7	(3,3)
A-036	Mandeyapecua	Petaca Fm.	34-23	-19.3608	-63.0749	324.5	84.3	(3,3)
A-038	Charagua	Yecua Fm.	8.2-6.98	-19.3512	-63.1346	192.4	29.2	(2,2)
A-039	Charagua	Chaco Gp.	6.82	-19.3532	-63.1311	3.5	0.4	(3,3)
A-040	Mandeyapecua	Ichoa Fm. (Tacuru Gp.)	163-100	-19.3604	-63.0746	258.6	107.0	(3,3)
A-041	Charagua	Escarpment Fm.	323-299	-19.3518	-63.1450	35.2	0.1	(3,2)
A-042	Charagua	Iquiri Fm.	383-372	-19.3524	-63.1547	2.0	0.2	(3,1)
A-043	Charagua	Iquiri Fm.	383-372	-19.3534	-63.1530	4.6	0.8	(3,3)
A-044	Charagua	Taiguati Fm.	330-315	-19.3519	-63.1460	8.5	3.2	(3,2)
A-045	Mandeyapecua	Chaco Gp.	6.98	-19.3633	-63.0809	6.2	1.0	(3,3)
A-046	Mandeyapecua	Yecua Fm.	8.2-6.98	-19.4203	-63.0737	2.9	0.8	(3,3)
A-047	Charagua	Ichoa Fm. (Tacuru Gp.)	163-100	-19.3539	-63.1653	54.6	19.7	(3,3)
A-048	Charagua	Chaco Gp.	~ 8-7	-19.3610	-63.1733	4.3	2.8	(3,3)
A-049	Charagua	Chaco Gp.	~ 8-7	-19.3545	-63.1715	24.8	4.9	(3,3)
A-050	Charagua	Chaco Gp.	~ 8-7	-19.3631	-63.1750	8.8	2.2	(3,2)
A-051	Borebigua	Chaco Gp.	8.57	-19.3710	-63.2307	3.6	0.4	(3,3)
A-052	Borebigua	Chorro Fm.	359-323	-19.3908	-63.1924	7.1	0.6	(3,2)
A-053	Borebigua	Chaco Gp.	~ 10-9	-19.3730	-63.2150	3.9	2.6	(3,3)
A054	Borebigua	Iquiri Fm.	383-372	-19.3721	-63.1916	3.1	0.6	(3,3)
A-055	Borebigua	Ichoa Fm. (Tacuru Gp.)	163-100	-19.3724	-63.2127	192.1	85.4	(3,2)
A-057	Borebigua	Escarpment Fm.	323-299	-19.3950	-63.2002	7.8	5.5	(3,2)
A-059	Borebigua	Escarpment Fm.	323-299	-19.4514	-63.1841	31.7	8.0	(3,3)
A-101	Borebigua	Tupambi Fm.	359-331	-19.4530	-63.1807	6.0	4.4	(3,3)
A-156	Carohuaicho	Escarpment Fm.	323-299	-19.2542	-63.3404	35.0	18.2	(3,2)
A-157	Carohuaicho	Chorro Fm.	359-323	-19.2545	-63.3313	27.0	15.4	(3,3)
A-159	Borebigua	Escarpment Fm.	323-299	-19.3533	-63.2046	5.4	3.6	(3,3)
A-160	Carohuaicho	Iquiri Fm.	383-372	-19.1302	-63.3444	2.7	0.4	(3,2)
A161	Carohuaicho	Tupambi Fm.	359-331	-19.1310	-63.3456	4.2	0.6	(3,3)
A-163	Carohuaicho	Ichoa Fm. (Tacuru Gp.)	163-100	-19.3025	-63.3130	173.6	79.3	(3,3)
A-164	Tatarenda	Escarpment Fm.	323-299	-19.1356	-63.3119	5.0	4.2	(3,2)
A-167	Curuyuqui	Chaco Gp.	8.86	-19.4544	-63.3416	7.2	1.8	(3,3)
A-168	Curuyuqui	Chaco Gp.	8.86	-19.4358	-63.3455	65.0	42.9	(3,3)
A-171	Tatarenda	Chaco Gp.	9.01	-19.1913	-63.2622	2.2	0.8	(5,5)
A-197	Carohuaicho	Escarpment Fm.	323-299	-19.3004	-63.3207	61.6	32.5	(6,6)
A-200	Carohuaicho	Escarpment Fm.	323-299	-19.1722	-63.3447	3.6	2.0	(4,3)

Ascending stratigraphically, the samples corresponding to the Upper Jurassic-Lower Cretaceous interval, present heterogeneous individual ages of wide dispersion determined between 412.0 ± 24.7 Ma and 23.1 ± 1.4 Ma, in a similar way to the Oligocene-Miocene samples showing old individual AHe ages of 493.1 ± 29.6 Ma to 242.1 ± 14.5 Ma, and to the Miocene clastic samples presenting AHe ages between 1.9 ± 0.1 Ma and 221.6 ± 13.3 Ma. Finally, the Miocene samples corresponding to tuffs and tuffaceous sandstones present two dissimilar stratigraphic age-individual AHe age relationships, depending on their clastic-volcanic components, structural position and stratigraphic location. On one hand, there are samples with stratigraphic ages being older than their corresponding individual AHe ages (samples A-039, A-046, A-048, A-051, A-053, A-167, A-171). On the other hand, there is one sample whose stratigraphic age is equivalent to the individual AHe ages measured (sample A-045). In the latter case, the aforementioned analysis contributed, together with the U-Pb SHRIMP measurements on zircons included in this study, to the definition of timelines in the Miocene-Pliocene interval, representing important constraints in the development of the numerical t-T modeling and the dynamic characterization of the sub-Andean fold-and-thrust system.

4.4. Thermal history modeling

Integrating the thermochronological data set and the regional-specific geological knowledge of the study area, thermal histories were modeled (HeFTy®) for 14 samples corresponding to Devonian (4), Lower Carboniferous (3), Upper Carboniferous (4) and Upper Miocene (3) stratigraphic ages. In the case of the regional transect involving the structures of Curuyuqui-Carohuaicho, Tatarenda, Borebigua, Charagua and Mandeyapecua, we find t-T paths consistent

with both the multiple thermochronometers data and the geological model. Depending on the sample and the thermochronometers used (data measured), different combinations were taken into account considering AFT data (confined-track lengths and single grain ages) and/or AHe data (single grain ages). The combination of thermochronometers led to robust statistically supported t-T paths with AFT data providing precision through 60-110 °C, and AHe data giving information through 40-70 °C.

For all samples, 50.000 t-T paths have been tested against the data set (Fig. 4, Fig. S3). Possible responses combining the thermochronological data and geological knowledge are statistically expressed through goodness of fit (G.O.F) values of 50% and 5%, represented by Good or Acceptable t-T paths, respectively. It is important to state that the combination of thermochronometers from multiple grains modeled together or a closely defined t-T geological constraint, both situations leading to a solid integration of thermochronological and geological data, in general yield lower G.O.F values. In the case of the study area, the samples were modeled with as many thermochronometers and detailed t-T constraints as possible searching for a realistic scenario suitable for all the combined data. Altogether, t-T models reveal between 5 and 4425 good, and between 22 and 8938 acceptable t-T paths.

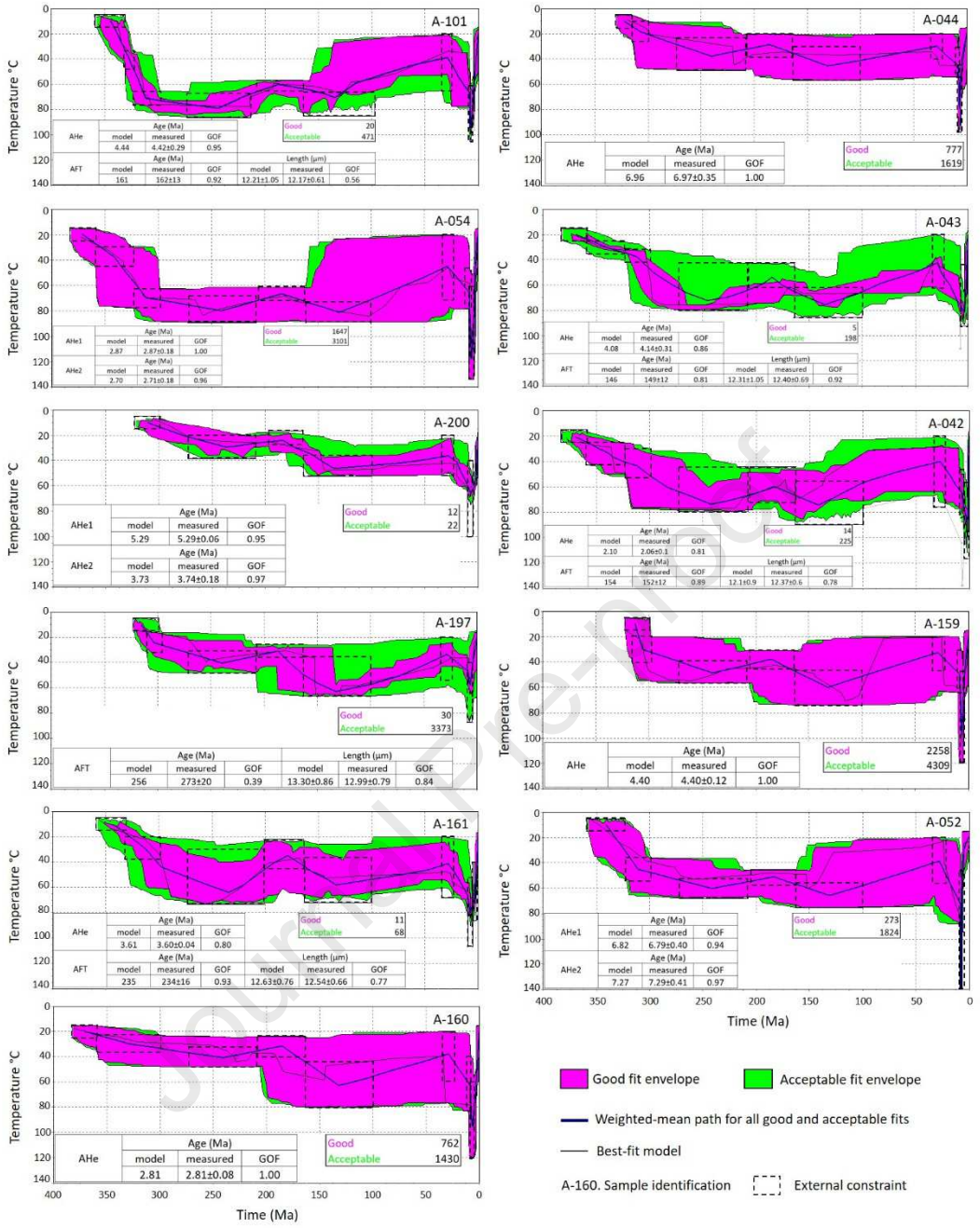

Fig. 4. Time (t)-Temperature (T)-evolution of the individual samples in the study area based on the combination of the thermochronological data set (AFT and/or AHe) and geological constraints with the software HeFTy® (Ketcham et al., 2007a, b). See t-T models location in Fig. 1C. Samples ordered according to their stratigraphic age (from older to younger) and structural location (from west to east), from bottom left to top right.

The numerical modeling performed in the study area reveals a complex thermal history from the Devonian until recent times giving place to the characterization of heating and cooling events, issues to be assessed in the petroleum system modeling. In this way, it was important to add as much detail as possible during t-T constraints definition on the one hand and to remain permeable to in principle unforeseen or illogical solutions that statistically adjust to the measured data, generating new working hypotheses to be deepened and tested, on the other. This occurs above all when it comes to geological events with undefined time and space parameters due to the lack of precise knowledge of the intervening variables.

4.5. Structural analysis. Balanced cross-section and shortening estimates

The structural analysis developed in the study area results from the combination of surface and subsurface data. The integration of mapping and stratigraphic survey data on the one hand, and the information corresponding to wells and seismic on the other, permitted developing the balanced cross section to be presented in this study (Fig. 5). Following the four-rheological-level model firstly applied by Hernández et al., (2018), the structural section developed and its corresponding restoration allowed to estimate a shortening value of 31 km, representing 33%, involving the structures of Curuyuqui-Carohuaicho, Borebigua, Charagua and Mandeyapecua.

The structural analysis in general, and the balanced cross-section constructed in particular, represented a key point as a suitable framework for analyzing the thermochronological data later integrated within the Upper Miocene to date chrono-kinematic modeling and interpretation.

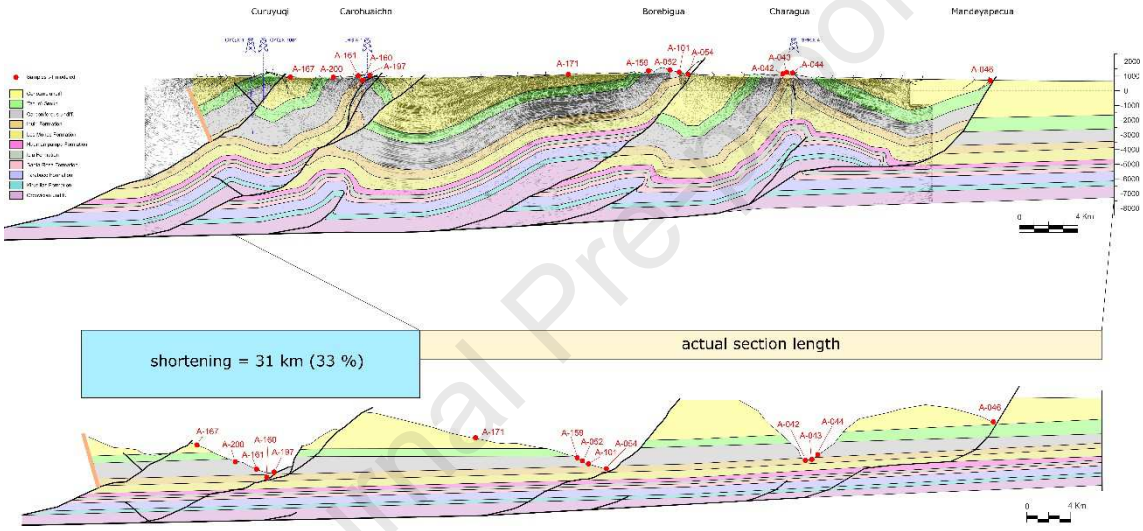

Fig. 5. Balanced cross-section built in the study area with the 2D seismic information (line BO90-05), wells, surface data (see location in Fig. 1 C), and its corresponding restoration. Vertical axis in meters below/above sea level. Samples t-T modeled projected onto deformed and restored cross sections (red dots).

5. Interpretation and discussion

The analysis of multiple thermochronometers and their combination with the geological knowledge for the development of evolutionary t-T scenarios (Fig. 4, Fig. S3), has led to an advance in the characterization of heating and cooling processes (timing, rates and magnitude), interpreted as subsidence-burial and exhumation-erosion phenomena, respectively. In this sense, the thermal history of the samples analyzed in the structural transect has been modeled, joining the structures of Curuyuqui to the west and Mandeyecua to the east, involving Devonian to Miocene stratigraphic units in the study area. The t-T models elaborated have made it possible to characterize the thermal phenomena that occurred from the Devonian until today, revealing a complex geological history.

All models show the t-T evolution since the corresponding depositional age until recent times (0 Ma). It is relevant to mention that the AFT data related to pre-depositional history is really scarce and related to very few samples, besides the partial annealing condition mentioned (e.g. Upper Carboniferous formation age, A-197 sample, with a P3 Precambrian population of

565.6±69.7 Ma, represented by 19.3% of the grains within the sample; or sample A-200, Upper Carboniferous in age with a P2 Lower Devonian population of 398±43.2 Ma, Table 3). In this way, we cannot be sure that each apatite grain comes from the same source with the same t-T evolution in order to analyze and interpret a pre-depositional history.

The geological model derived from the data acquired during 2016-2017 and the authors previously mentioned (published data) led to the geological evolution from Devonian times until nowadays in the study area. The model assumes a continuous subsidence-sedimentation heating-linked stage from the Upper Devonian up to the Upper Carboniferous-Permian boundary, applying the E-mode included in HeFTy® (E for Episodic) giving rise to the possibility of internal unconformities or sedimentation rates variation. This Upper Devonian to Upper Carboniferous-Permian boundary stage is followed by the assumed onset of sedimentation and subsequent erosion-linked cooling exhumation for the Permian-Triassic time, a stratigraphic interval that is regionally preserved but totally absent in the study area. Moving forward in time, the sedimentary record led to think about a new subsiding and sedimentation heating interval related to the Jurassic-Lower Cretaceous period, accommodation space driven possibly by extensional phenomena. It must be stated that an alternative scenario was designed considering an ongoing subsidence-sedimentation-heating stage from the Upper Carboniferous-Permian boundary until the Lower Cretaceous yielding no results, in concordance with the apatite fission-track results exposed. To test how the samples were influenced thermally in time by the Jurassic-Lower Cretaceous sedimentary column and the possible subsidence triggering processes, t-T models have been permitted to run loosely covering a wider temperature interval in relationship with mean and maximum thicknesses preserved within the basin (Tab. 1, Tab. S4) as well as possible geothermal gradient variations. From the Lower Cretaceous up to the Oligocene-Miocene limit, a possible cooling phenomenon took place leading to an important time-elapsed-unconformity, responsible for placing thin Oligocene-Miocene amalgamated paleosoil deposits of Petaca Formation directly on top of the aforementioned Mesozoic strata. From the Middle Miocene, the t-T evolution is dominated by the sub-Andean fold-and-thrust belt dynamics including extremely fast subsidence-exhumation processes (high heating-cooling rate phenomena, respectively), leading to the nowadays structural-tectonic configuration.

5.1. Devonian, Carboniferous-Permian to Triassic time

The t-T histories modeled for the study area suggest a long-term warming phenomenon from ~ 383-359 Ma (Upper Devonian) to ~ 245-240 Ma (Middle Triassic), associated with an interval of subsidence and sedimentation of the units belonging to the Upper Devonian (Iquiri Fm.), Lower and Upper Carboniferous (Machareti and Mandiyuti Groups, respectively) and Permian-Triassic (Cuevo Group) reaching maximum variable temperatures of 40 - 80 ° C. The numerical modeling carried out on the Devonian samples, located in the structures of Carohuaicho (A-160), Borebigua (A-054) and Charagua (A-042 and A-043), reflect that said thermal variability is fundamentally related to the Carboniferous units. The isopach maps developed by Hernández et al., (2018) (Fig. 3) and the seismic information presented by Viera and Hernández, (2001), and Rousse et al., (2018), complemented by the mapping and stratigraphic survey tasks for the years 2016-2017, show important variations in the Carboniferous units on both a regional and local scale. The study area reflects thickness variations in both east-west and north-south directions. In the first case, thicknesses of ~ 1,000 meters are evident in the anticline structure of Charagua (eastern sector of the study area, with complete Carboniferous record clearly defined by its lower contact with the Devonian and its upper contact with the Jurassic-Lower Cretaceous), values of ~ 1,800 meters in the Borebigua structure (complete stratigraphic thickness), and to the west a thickness of ~ 1,120 meters in the Carohuaicho anticline. In the second case, the Carohuaicho structure exhibits thicknesses of ~ 500 meters in the northern

sector of the study area doubling its thickness towards the southern sector with ~ 1,120 meters over a distance of 40 kilometers, while the Borebigua structure shows a thickness increase in reverse with values of ~ 1,520 meters in the southern sector and values greater than ~ 1,800 meters in its northern sector over a distance of 30 kilometers. The variation in thickness identified in the work area and at the regional scale allows inferring the existence of differential subsidence phenomena, pointing to the formation of different Carboniferous-age depocenters, suggesting a northwest-southeast arrangement (Hernández et al., 2018), as pointed out by the Eohercinian orogeny deduced by palynological mapping in Chaco plain (Suarez Soruco and Lobo Boneta, 1983). The analysis of the Carboniferous units in a regional sense also reflects variations in the age of their basal deposits from Tournaisian-Visean to Westphalian-Stephanian, developed erosive discordance by, on different terms of the underlying Devonian units (~ Upper Givetian to Strunian age). On the other hand, the fluvial and glacial-marine deposition environment interpreted for the Carboniferous units suggests sedimentation processes with internal erosions and changes in their sedimentation rates associated with base-level fluctuations (Viera and Hernández, 2001) and showing sedimentary deformation of variable scale suggesting instability of sediments in sectors with sloping substrates.

Coincidentally with what is observed in the isopach maps referenced, wells and seismic data, and outcrop information, the t-T trajectories defined for the Devonian and Carboniferous samples in the study area exhibit changes in slope, showing variable subsidence rates in the Lower Carboniferous and Upper Carboniferous, depending on the position analyzed (Fig. 4) with values ranging between 0.01 mm/year and 0.1 mm/year (average, 0.03 mm/year. Fig. 6). In this case, it is important to mention the existing problem in determining the precise age of Carboniferous deposits, generally associated with scattered palynological data.

The thermal history developed from thermochronological data and the applied geological constraints suggest that, after the mentioned Carboniferous interval, the subsidence and deposition of the Permian-Triassic units (Cuevo Group, Cangapi and Vitiacua formations) took place. This time interval is regionally represented by clastic deposits (fluvial and aeolian) and marine carbonates, under warm climate conditions, a paleoclimatic situation possibly started in the Lower Permian (Gallo, 2019). This interval of the t-T evolution is visualized in the developed models as a low subsidence time segment with a rate ranging between 0.004 mm/year and 0.02 mm/year (average, 0.01 mm/year. Fig. 6), in coincidence with the ~150 meters thick preserved deposits in the northern plunge of the Aguaragüe structure. The application of thermochronological analysis in the structures of Charagua, Borebigua, Tatarenda and Carohuaicho allowed the generation of precisions regarding the deposition and subsequent exhumation/erosion of the Cuevo Group, a unit not preserved in the stratigraphic record of the area with the exception of its southern end. Then, from the development of the aforementioned numerical models, a segment of geological history could be reconstructed, characterizing a time interval not preserved as a rock unit. In this sense, the deposits corresponding to the Upper Jurassic-Lower Cretaceous lie directly on Carboniferous units.

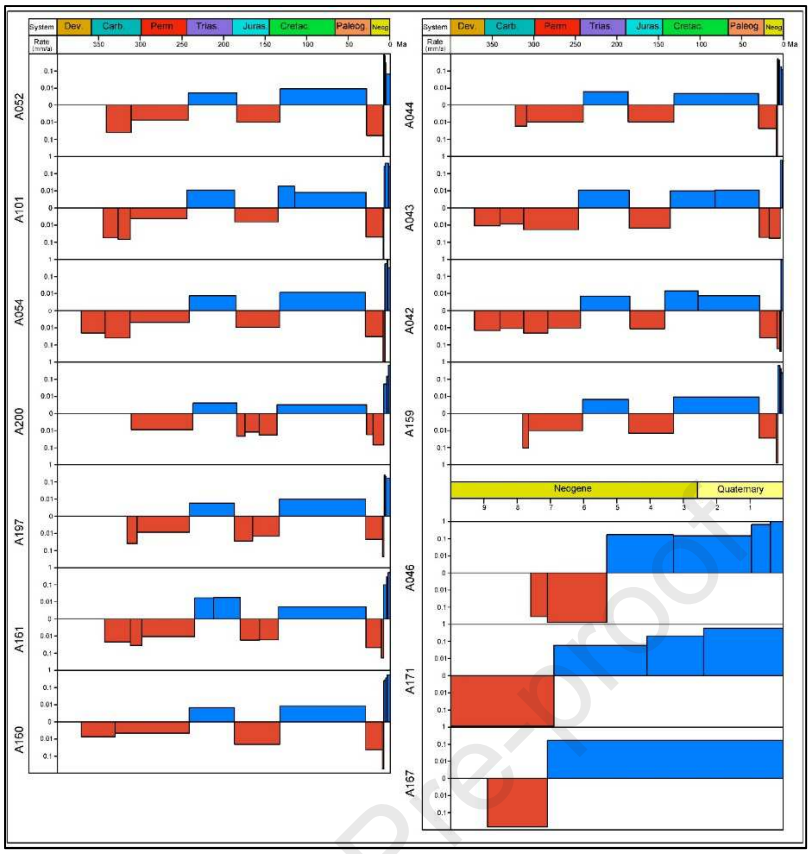

Fig. 6. Calculated exhumation and subsidence rates, derived from combined geochronological and thermochronological t-T-modeling of the thermal evolution of individual samples in the study area (Fig. 4, Fig. S3). Blue bars indicate exhumation (derived from cooling rates), red bars signify subsidence (derived from heating rates). The thickness of the bars implies higher/lower rates.

5.2. Permian and Triassic, cooling and exhumation/erosion

As mentioned previously, the Permian-Triassic interval does not have physical expression in the sedimentary record in the work area. At the regional scale, the analysis of thicknesses of this time interval suggests the existence of zones of variable subsidence with values of preserved thickness ranging between 50 meters and 580 meters, with a general decrease from the southwest to the northeast, with a possible alignment of minor depocenters with this same distribution (Hernández et al., 2018), possibly associated with extensional phenomena that occurred during the late Paleozoic and Mesozoic time (Sempere et al., 1998).

The modeling of the t-T trajectories developed for the Devonian and Carboniferous samples in the study area suggest a cooling phenomenon of ~ 9 °C to 11 °C possibly associated with the exhumation and erosion of the entire Cuevo Group and the upper portion of the Carboniferous (~ 300-350 meters in magnitude), starting at ~ 245-240 Ma (Middle Triassic) and ending at ~ 188-185 Ma (Lower Jurassic), with an average exhumation rate of 0.01 mm/year (Fig. 6). In coincidence with the latter, in all the control points surveyed in the study area, aeolian and fluvial deposits from the Upper Jurassic to the Lower Cretaceous (Tacurú Group) are identified overlying, important unconformity in the middle, on top of Upper Carboniferous units. Therefore, the exhumation event mentioned would explain the absence of deposits from the Upper Carboniferous to Lower Permian (Mandiyuti Group, San Telmo Formation) and from the Permian to Triassic (Cuevo Group, Cangapi and Vitiacua Formations) in the area. It is interesting to mention that, in the process of developing the numerical modeling for the

Devonian and Carboniferous samples, an attempt was made to simulate a continuous subsidence/heating phenomenon involving the Carboniferous, Permian-Triassic and Jurassic-Cretaceous intervals, that is, without intermediate cooling/exhumation processes, and no result was obtained.

5.3. Lower Jurassic to Lower Cretaceous

The beginning of the deposits corresponding to the Jurassic-Cretaceous in the southern sub-Andean region of Bolivia starts from 181.5 ± 0.9 Ma (Kusiak et al., 2014), a timeline corresponding to the dating of the Entre Ríos Basalt (Fig. 2), a volcanic interval of volumetric importance and of great regional distribution, with a crustal component chemical signature. The base of the Tacurú Group in the study area has been determined by its fossil content as Upper Jurassic to Lower Cretaceous (Carvalho, 1993, 1996, 2001, 2014; Carvalho and Srivastava, 1996; Carvalho et al., 2002; Suarez Riglos and Carvalho, 2018). The thickness analysis corresponding to this interval (Hernández et al., 2018), suggests an extremely different distribution and thickness variations when compared to the intervals stratigraphically below, suggesting different accommodation space generation mechanisms. In this sense, there is a general trend of increasing thickness to the west of the sub-Andean system as a stepped differential subsidence, generating an irregular substrate with variable accommodation space. On the other hand, the aforementioned east-to-west general trend presents minor accommodation variations, giving place to elongated depocenters with major axes of north-south to northeast-southwest orientation. The latter contributes to the compartmentalization of the Jurassic-Cretaceous basin in rhomboidal zones, suggesting extensional mechanisms with a dextral strike-slip component, forming a transtensional basin (Hernández et al., 2018).

The Lower Jurassic-Lower Cretaceous interval represented by aeolian-fluvial deposits of the Tacurú Group in the southern sub-Andean region of Bolivia, presents thickness variations between 80 meters and 1,550 meters with higher frequency values in the 700-800-meter interval (Hernández et al., 2018). In the study area, these deposits are represented from east to west by thicknesses of ~ 900 meters, ~ 750-850 meters and up to ~ 1,200 meters, in the positions of Charagua, Borebigua and Carohuaicho. Contrary to the aforementioned increase in thickness from north to south for the Carboniferous interval in the Carohuaicho position, the Jurassic-Cretaceous interval shows a decrease in thickness in this sense to values of ~ 655 meters in the southern tip of the area, which would be associated to different accommodation space generation mechanisms when the Carboniferous and the Jurassic-Cretaceous intervals are compared (Hernández et al., 2018).

The t-T models show an important subsidence/burial heating-linked stage of the Jurassic-Cretaceous deposits between ~ 180-135 Ma reaching temperatures of ~ 75-80°C (subsidence rate ~ 0.01-0.03 mm/year) and a subsequent smooth cooling phenomenon between ~ 140-130 Ma and ~ 34-23 Ma to surface temperatures close to ~ 20°C (Figs. 4, 6), marking a sharp asymmetric heating-cooling path. It is important to mention that the weighted-mean path as well as the best-fit one of the Carboniferous samples located in the Carohuaicho structure (A-197), exhibits temperatures reached of ~ 63°C, even though lower temperature conditions are possible as it is shown in the corresponding t-T model, evidencing thermal values 13°C higher than estimated from the preserved thickness and the normal geothermal gradient used of 30°C/km, suggesting a $\Delta T/\Delta z$ variation close to 33°C/km. The final section of the subsidence stage and the start of the subsequent cooling could represent an indication to limit the age of the top of this stratigraphic interval, coinciding with the existing dating in Brazil and correlated in Argentina and Uruguay with basaltic effusions (Paraná-Etendeka flood basalts, 133.0 ± 1.0 Ma, ($^{40}Ar/^{39}Ar$) (Renne et al., 1992, 1996, Basalto de Sierra Geral Formation) above the aeolian-

fluvial interval of the Botucatú Formation, equivalent to the Tacurú Group in Bolivia. On the other hand, this definition allowed specifying the time lapse of no record associated to the unconformity between the Tacurú Group and the overlying Petaca Formation estimated at ~ 100 Ma between the Lower Cretaceous and the Oligocene-Miocene. Apatite fission-track ages determined for the Devonian and Carboniferous samples in the study area show a wide range of single grain ages (Tab. 3), suggesting a partial annealing condition for the samples analyzed, which would be consistent with maximum temperatures reached during the Upper Jurassic-Lower Cretaceous interval around ~ 80°C as shown in the t-T models performed.

5.3.1. Upper Cretaceous-Eocene, extensional basins thermal influence? to Oligocene-Miocene boundary

The Upper Cretaceous-Eocene interval represents a particular case with no stratigraphic record preserved in much of the southern sub-Andean system of Bolivia, and the study area presented here is no exception. As discussed in section 5.3, there is a ~ 100 Ma time gap between the Lower Cretaceous and the Oligocene-Miocene, not preserved in the rock record. However, to the west in the Eastern Cordillera and the Altiplano, in the northern end of the southern sub-Andean, in the northern sub-Andean of Bolivia, and in the southern extreme of Bolivia-northwestern Argentina, there are preserved deposits corresponding to the Upper Cretaceous to Eocene interval (De Celles et al., 2011; Hernández et al., 2017; Constantini et al., 2018). In this sense, in the area of the Eastern Cordillera and Altiplano between the Upper Cretaceous and the Eocene, important basins with marginal marine influence and carbonate lakes developed together with incipient continental deposits (Sempere et al., 1997). These basins, linked to extensional phenomena, include those of the El Molino and Santa Lucia Formations, developed in Potosí, Chuquisaca and Cochabamba, making up what it is known today as the Eastern Cordillera and southern Altiplano of Bolivia (Lamb and Hoke, 1997). These basins are named as Camargo, Miraflores, Tarapaya, Maragua, Toro Toro basins, etc. On the other hand, towards the central portion of the sub-Andean fold-and-thrust belt, there are river and brackish lake deposits of the Maastrichtian age corresponding to the Yantata and Cajones formations (Oller and Franco, 1981; Gutierrez & Marshall, 1994), while towards the northern extreme of the northern sub-Andean system in Bolivian, shallow water deposits and overlapping paleosoil levels, assigned to the Eslabón and Flora formations, are preserved. Finally, towards the southernmost edge of Bolivia and northwestern Argentina, the intra-continental rift basin of the Salta Group develops between the Lower Cretaceous (~115 Ma) and the Eocene (~ 40 Ma), with well-defined tectonic and thermal subsidence stages, totaling more than 2000 meters thick preserved, with basaltic effusions and tuffaceous levels contributing to the chronostratigraphic analysis (Hernández et al., 2017). Taking into account the aforementioned, it is possible that, despite the absence of deposits corresponding to the Upper Cretaceous – Eocene time in the sub-Andean area, the thermal phenomena linked to extensional processes might have influenced the t-T evolution of previously deposited units. On the other hand, some authors have presented evidence of an already acting compressive dynamics for the Paleocene to Eocene time in Bolivia and northwestern Argentina (Sempere et al., 1997; De Celles et al., 2011), giving place to a complex geological scenario.

The contact between the fluvial deposits with intense development of Oligocene-Miocene edaphic processes of the Petaca Formation on top of the aeolian-fluvial deposits of the Jurassic-Lower Cretaceous Tacurú Group is represented by a regional unconformity estimated of ~ 100 Ma (See Section 5.3). The low thickness of the deposits above the aforementioned unconformity of up to ~ 100-130 meters thick in the study area, and the presence of overlapping paleosoils are indications of a time interval of low subsidence and low sedimentation rate, under temperature conditions with values close to surface (~ 20°C; Rosario et al., 2008, 2017). This low

sedimentation rate interval could possibly be related to a ~ 20-30 Ma forebulge position at the latitude of the study area being coherent with the Eastern Cordillera main uplift defined for the same time interval (Kennan et al., 1995; Lamb and Hoke, 1997; Horton, 1998; Anderson et al., 2018). Similar intervals have been associated to forebulge positions for the Paleocene-Eocene times in northwestern Argentina (De Celles et al., 2011; Horton 2018). The t-T models developed in the Devonian-Carboniferous samples from the Carohuaicho, Borebigua and Charagua structures suggest a gentle cooling/ exhumation interval between ~ 140-130 Ma and ~ 34-23 Ma with an exhumation rate of ~ 0.003-0.018 mm/year (Fig. 6). It is important to mention that the cooling/exhumation period evidenced between the Tacurú Group and the Petaca Formation requires a more in-depth analysis from obtaining more thermochronological and provenance data, evaluating the possibility of internal unconformities within the Tacurú Group and specifying the thermal history between ~ 130 and ~ 34-23 Ma, including the existence of possible intermediate thermal phenomena.

5.4. Miocene to recent times, sub-Andean fold-and-thrust belt dynamics

The sub-Andean system constitutes a fold-and-thrust belt with a complex space-and-time dynamic characterized by both in-sequence deformation events and out-of-sequence phenomena with a general east-southeast to east-northeast vergence depending on the latitude. In addition, a strike-direction diachronism is noted with respect to the structures growing time according to the analyzed sub-Andean segment, south, central or north (Hernández et al., 2002; Hernández et al., 2017; Anderson et al., 2018; Constantini et al. 2018). The analysis of the structural growing ages in the southern sub-Andean published by Hernández et al. (2002) and Anderson et al., (2018) suggests, despite the interpretative differences regarding the dynamics of the fold-and-thrust system, a migration of the deformation beginning in the sub-Andean environment at ~ 11-8 Ma and with ages of ~ 3-1.5 Ma for structures located towards the eastern end. The results obtained in the study area show the growth of the structures of Curuyuqui, Carohuaicho, Tatarenda, Borebigua, Charagua and Mandeyapecua, that is, all the structures identified, between ~ 7.1 Ma and ~ 3-2.5 Ma. The developed t-T models (Figs. 4, 7) and the apatite (U-Th-Sm)/He ages (Tab. 5, Tab. S3) obtained for the Devonian, Carboniferous and Miocene samples allowed to establish the onset of the erosion-linked cooling phenomenon related to structural growth at ~ 7.1-6.6 Ma (Curuyuqui-Carohuaicho), ~ 7-6.4 (Borebigua), ~ 7 Ma (Charagua), ~ 5.2 Ma (Mandeyapecua), and ~ 3-2.5 Ma (Tatarenda) (Figs. 7-8). In the latter structure, it is possible that a really smooth cooling phenomenon could have taken place between ~ 6.8 Ma and ~ 3 Ma in relationship with Borebigua structural growing age. The structural timing of Carohuaicho and Borebigua was also reproduced through thermo-kinematic modeling by Cristallini et al., (2020, this volume) and Hernández et al., (2020), respectively, obtaining comparable results. This scenario implies a slightly diachronic initial growing time for the structures of Curuyuqui-Carohuaicho, Borebigua and Charagua, and a clearly later growth for the Mandeyapecua and Tatarenda structures (Fig. 8). The registered growth is linked to the generation of structures detaching in ductile intervals of Rheological Level 1 (RL 1, Hernández et al., 2018) and modeled as propagation folds by Trishear (with the exception of the Mandeyapecua structure related to a shortening transferred from RL 1 to RL 3, Los Monos Formation). This kinematics results consistent with the rheology of the fine-grain material that makes up the Silurian and Ordovician sediments. The growing time relationships recorded between structures suggest a moderate efficiency of the mentioned detachment level, allowing the shortening transfer, and generating a spacing between structures of ~ 8-16 km at ~ 7-5 Ma. On the other hand, the (U-Th-Sm)/He single-grain ages exhibit a high frequency between ~ 5.3 Ma and ~ 1.2 Ma, making it possible to reconstruct the most recent chrono-kinematic history for the study area. In this sense, the integration of the thermochronological results, the constructed

t-T models and the developed structural analysis allowed to deduce that the aforementioned young ages are linked to the recent history of folding-faulting (e.g. Charagua and Mandeyapecua structures), to out-of-sequence movements affecting the back-limb of already formed structures (e.g. Carohuaicho and Borebigua cases), or fault-related folds posthumously formed when compared to the general structure (e.g. Tatarenda anticline), as the shortening of the fold-and-thrust system increases. The spacing between structures is controlled by the lower detachment level and subsequently distorted by the appearance of the out-of-sequence structures. In this way, the spacing between structures before the development of the out-of-sequence ones, that is 8 to 16 km, it is consistent with the magnitude analyzed by Rocha and Cristallini (2018) and Hernández et al., (2018).

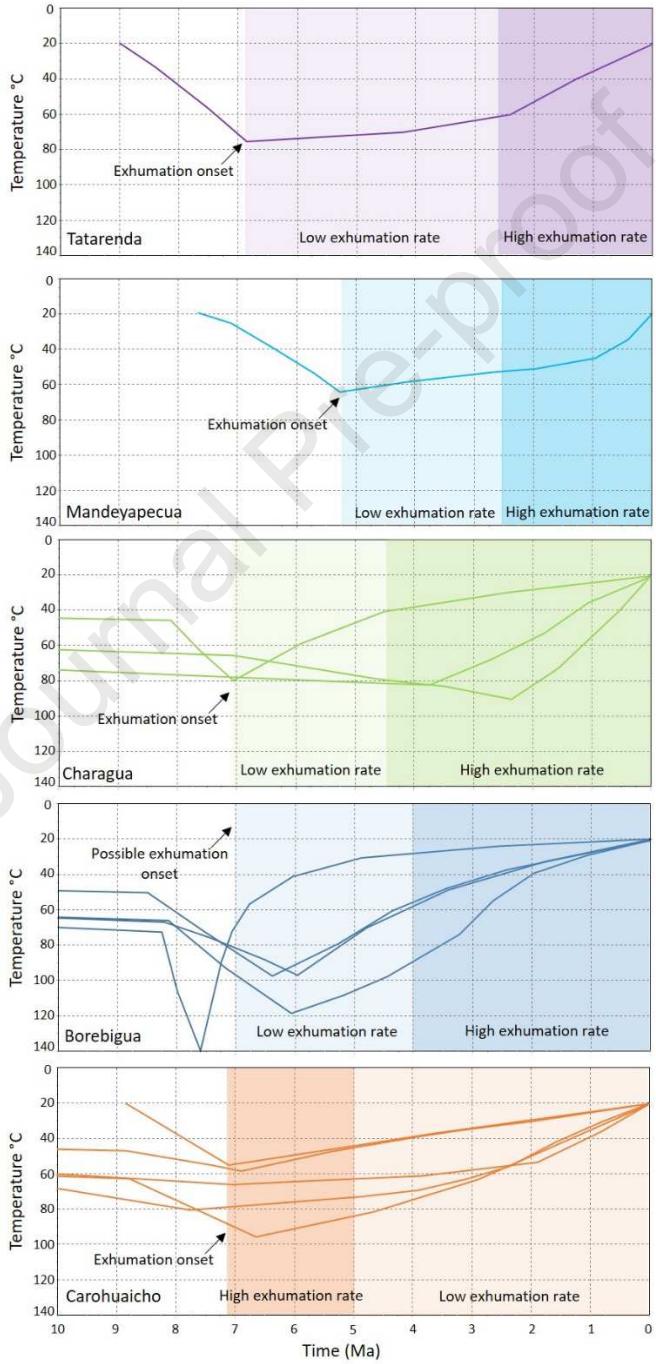

Fig. 7. Upper Miocene Time (t)-Temperature (T)-evolution showing the weighted mean paths for all the samples modeled in the study area. Carohuaicho structure (samples A-160, A-161, A-197, A-200, A-167),

Borebigua structure (samples A-052, A-054, A-101, A-159), Charagua structure (A-042, A-043-, A-044), Mandeyapecua structure (sample A-046), and Tatarenda structure (sample A-171). Shaded rectangles represent the growing time interpreted for each structure based on AHe ages and t-T modeling.

The plant-view analysis of the structures identified in the study area suggests an advance of the deformation towards the east of greater magnitude with respect to the positions analyzed further south by Anderson et al., (2018) and Hernández et al., (2002). This situation is consistent with an increase in the shortening values from south to north with magnitudes of 30-36% in the Argentina-Bolivia international border (Hernández et al., 2002) and values close to 50% at the latitude of the Pilcomayo river (Dunn et al., 1995). The total shortening value determined for the study area reaches 33% (Figs. 5, 8) showing a west-to-east decrease. In this sense, the shortening magnitude involving the structures of Carohuaicho to Borebigua reaches up to 45-51% while the structures to the east, Charagua and Mandeyapecua, present values around 26 %, which is consistent with growing an east-verging system. This scenario shows that the aforementioned shortening increase from south to north would be specially linked to the structures to the west as shown by Sanchez et al., (2020), having estimated a shortening of 40 % for the whole sub-Andean system. On the other hand, a count of the structures plunging to the south in comparison with the northward plunging structures in the southern sub-Andean (from the study area to the Argentina-Bolivia international border), results in a wide 32-to-17-difference in favor of the southward plunging structures, which is coherent with a south-to-north shortening increase. From a regional point of view, the Bolivian Orocline appears as a complex system with greater shortening values in its central portion (Kley et al., 1999; Arriagada et al., 2008) in coincidence with the axis of topographic symmetry characterized by Gephart (1994) and modeled by Capitanio (2011). This scenario is accompanied by a generalized symmetry in the development of counterclockwise and clockwise rotations, to the north and south of the aforementioned symmetry axis, respectively, supported by both paleomagnetic evidence (Rousse and Gilder, 2005; Arriagada 2008) and GPS station data (Allmendinger et al., 2005). The previously mentioned shortening variations for the southern sub-Andean and the greater advance of the deformation front in the study area, is related to a north-south diachronism in the growth age of the structures. This is evidenced by older ages to the north with exhumation phenomena concentrated at ~ 7-5 Ma for the study area, and ages of ~ 6-3.5 Ma determined by Anderson et al., (2018) to the south for strike-equivalent structures. The high frequency of apatite (U-Th-Sm)/He averaged ages concentrated in ~ 4-3 Ma published by Anderson et al., (2018) in the structures of Suaruro, Mandiyuti and San Antonio, and the ages of ~ 2-1 Ma in the Aguaragüe structure would be linked to the recent structuring of the fold-and-thrust belt in this position as a result of an increase in the accumulated shortening of the system. This match with the out-of-sequence deformation stage documented by Hernández et al., (2002) and Echavarria et al., (2003) from ~ 4.5 Ma in northwestern Argentina. On the other hand, it is interesting to mention that the north-south diachronism mentioned in terms of the structural timing comparing Charagua, Borebigua and Carohuaicho to the north (~ 7-5 Ma, this study) and Aguaragüe, San Antonio, and Mandiyuti-Suaruro to the south (~ 6-1 Ma, Anderson et al., 2018), it might not be gradual but rather abrupt, which postulates a considerable relevance for the transfer zone over which the Cuevo river currently runs (Fig. 1B). The transfer zone mentioned is expressed either by plunging structures or by along-strike changes or inflections.

5.4.1. Chrono-kinematic evolution, 7.1 - 0 Ma

The recent sub-Andean dynamics in the analyzed transect is characterized by processes of subsidence and subsequent exhumation experienced by the samples analyzed, generating a

complex thermal history. The developed models suggest a variable t-T history depending on the analyzed structure. In this sense, there is evidence of a subsidence phenomenon experienced by the samples linked to the lithostatic load corresponding to the deposits prior to the growth of a structure (pre-growth strata). This subsidence is characterized by two intervals with clearly differentiable rates; a low-subsidence rate interval (average ~ 0.05 mm/year) linked to the west-east basal diachronism of the Miocene deposits in the sub-Andean setting (Hernández et al., 2002; Echavarría et al., 2003) with extreme ages of 24.4 ± 1.3 Ma (western edge, inter-Andean-sub-Andean boundary; Erikson, 1998) and 6.98 ± 0.31 Ma (eastern end, Mandeyapecua structure, this publication), and an interval of higher subsidence rate (average ~ 0.6 mm / year, Fig. 6) linked to the lithostatic load of the adjacent structures already developed and the sediments supply due to their erosion. This higher subsidence rate interval is related to maximum accumulated thicknesses of ~ 2500-3000 meters (Tab 1, Tab. S4) which would lead to temperatures around ~120°C. Nevertheless, the time associated with these temperature conditions, as displayed by the t-T history models performed, would not have been enough to completely anneal-reset the AFT system as it is defined by Gleadow and Duddy, (1981) with temperature and time period values of ~ 110°C/10 Ma. On the contrary, the temperature conditions mentioned led to a complete reset of the apatite (U-Th-Sm)/He system overpassing the reference closure temperature and time period of ~70°C/1 Ma. It is relevant to comment that geothermal gradient values being lower than 30°C/km were tested for the Upper Miocene interval by Cristallini et al., (2020, this volume) and Hernández et al., (2020), yielding equivalent results. Finally, the developed models suggest exhumation processes of considerable speed between 7.1 Ma and 0 Ma. This phenomenon is associated to the growth of the structures identified in the area, with average values of ~ 0.5 mm/year, presenting maximum values of ~ 0.9-1.3 mm/year (Figs. 6-7).

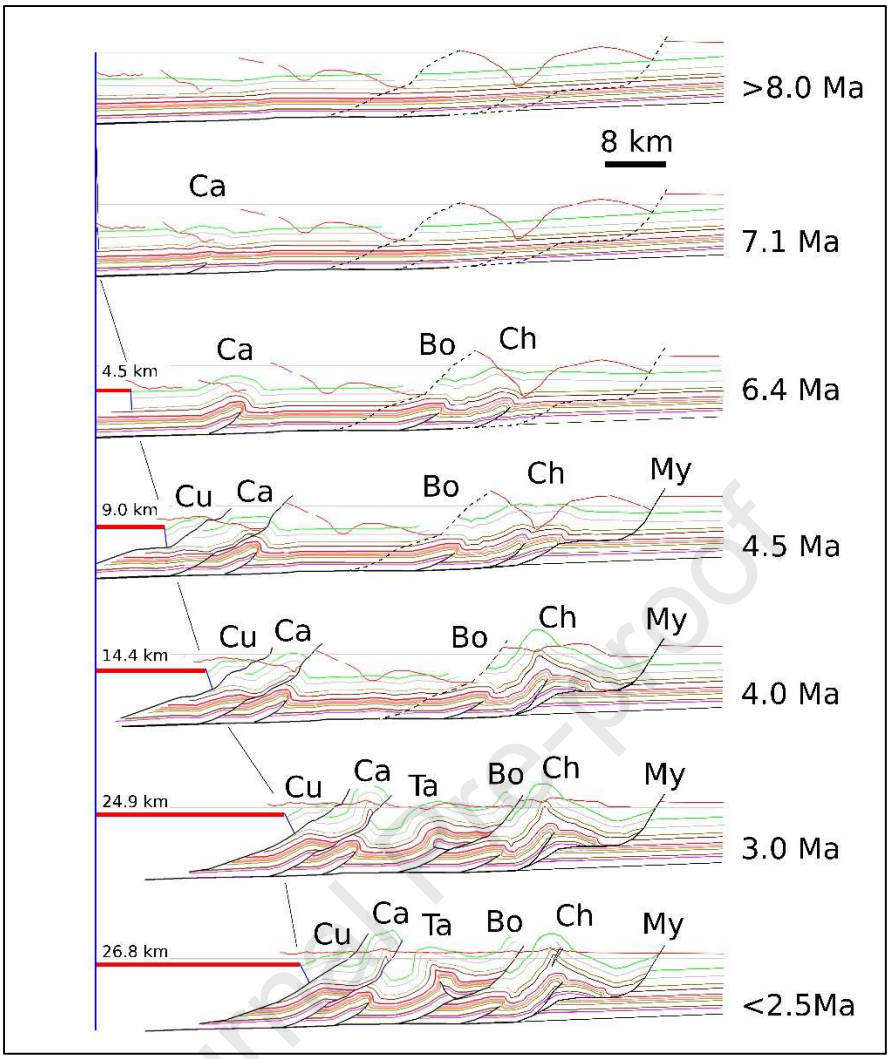

Fig. 8. Chrono-kinematic evolution of the study area, from > 8 Ma to 0 Ma, based on the thermochronological data set and t-T numerical modeling (See location in Fig. 1 C). Red bars indicating shortening magnitude (total shortening estimated: 33 %).

The analysis of exhumation rates carried out in the Carohuaicho, Borebigua and Charagua structures, taking into account the stratigraphic thickness between samples and the results obtained by apatite (U-Th-Sm)/He, shows that the Carohuaicho structure begins its growth at high speed (~ 1.2-1.6 mm/year) between ~ 7 Ma and ~ 5 Ma, while the structures of Borebigua and Charagua show low exhumation rates for this interval with values of ~ 0.2-0.3 mm/year. At 5-4 Ma, the Carohuaicho structure notably decreases its exhumation rate to values close to ~ 0.3 mm/year, transferring shortening to structures located to the east, Borebigua and Charagua, and generating the Mandeyapecua structure. The AHe-ages and the t-T trajectories emerging from numerical modeling denote a significant growth rate at ~ 2.5-3.5 Ma with average values of ~ 0.5-0.6 mm/year and maximum values close to ~ 1 mm/year, for the structures of Charagua, Borebigua and Mandeyapecua. It is in this generalized shortening interval that the growth of the westward- verging structure of Tatarenda becomes noticeable from ~ 2.4 Ma, with an exhumation rate of ~ 0.5-0.6 mm/year. The latter induced almost total erosion of the Miocene deposits above the sample located on the axis of the syncline between Tatarenda and Borebigua (Itaí), which is consistent for the structurally high position interpreted for said syncline.

The integration of thermochronological results and the developed structural analysis allowed to reconstruct the chrono-kinematic history of the study area (Fig. 8). This led to characterize the

space-and-time evolution of the fault-related anticline structures, representing the main objective in conventional reservoirs, and therefore, the evolution of traps as a component in the oil and gas system.

6. Oil and Gas system perspectives

The development of the Oil and Gas thermal history modeling performed for the syncline located between Charagua and Borebigua structures (1D Petromod®, 2012; Fig. 9, Figs. S5-S6; see location in Fig. 1C) permitted evaluating the possible source rocks in the area as described by Cruz et al., (2002, 2008): a) Emsian-Eifelian-Givetian interval (Los Monos Formation), b) Lochkovian interval (fine-grain sediments within the Santa Rosa Formation) and c) Silurian interval (Kirusillas Formation). The integration of thermochronological data and numerical modeling in the Charagua structure (Upper Devonian Iquiri Formation) was the key point to define the maximum temperature reached by the potential source rocks evaluated and the structural timing of the fault-related anticline (conventional target trap).

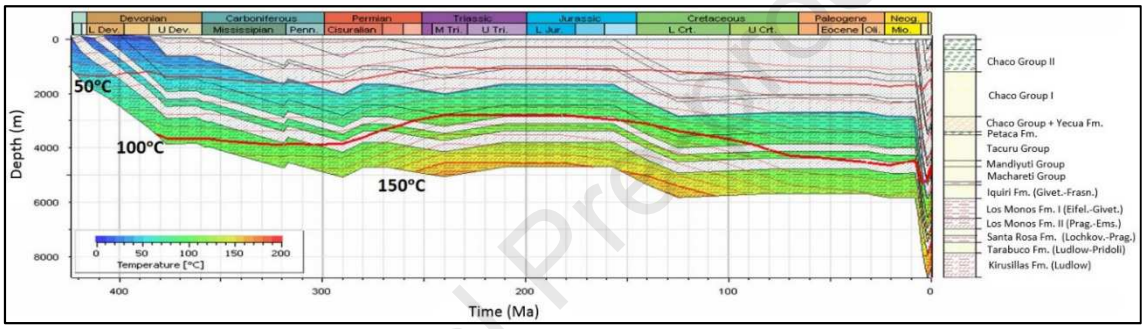

Fig. 9. Thermal history model (Petromod® 2012-1D) developed in the study area. Burial curve with temperature values for the source-rock intervals in the study area: Los Monos, Santa Rosa (fine-grain interval), and Kirusillas Formations. See location in Fig. 1C.

With the processing of the data, the following results were obtained for the already mentioned source rocks (Figs. S6-7):

a) Emsian-Eifelian-Givetian interval (Los Monos Formation)

-Ro values estimated from 0.8% to 0.71%
-Transformation Relationship (TR): from TR 37% to 16% (at the current time).
-Total mass generation (Emsian): of 0.6 Mton. (at the current time). Expulsion total mass: 0 Mton. (at the current time).
-Maturity perspectives: immature generating rocks.

b) Lochkovian interval (fine-grain sediments within the Santa Rosa Formation)

-Ro values estimated from 1% to 1.1%.
-Transformation Relationship (TR): 75% (at the current time)
-Total mass generation: 1.5 Mton. (at the current time). Expulsion total mass: 0.9 Mton. (at the current time).
-Maturity perspectives: source rocks in oil and gas generation window.

c) Silurian interval (Kirusillas Formation)

- Ro values estimated of 1.28% to 1.51%.

-Transformation Relationship (TR): of 96% (in the Lower Triassic).
-Total mass generation 0.82 Mton. (at the current time). Expulsion total mass: 0.81 Mton. (in the Upper Triassic).
- Maturity perspectives: source rocks in final stage of gas generation to overmature.

7. Conclusions

The evolution of fold and thrust belts requires time data restrictions to determine the rates related to the interaction of surface and subsurface processes and to quantify the time involved in the components of the petroleum system: reservoir, seal, source rock and trap. The sub-Andean fold-and-thust belt in the Bolivian territory in general, and the transect that links the structures of Curuyuqui-Carohuaicho-Tatarenda-Borebigua-Charagua and Mandeyapecua in particular, constitutes a complex multi-variable system in which the definition of t-T trajectories has led to new suitable structural and stratigraphic conclusions.

The integration of multiple thermochronological and geochronological systems (AFT-AHe-UPb) and the existing surface and subsurface geological constraints, made it possible to develop a chrono-kinematic characterization of fault-related anticlines, defining their formation chronology, structural growth rate and a link between them in the study area. In this sense, the thermochronological data set and the geological constraints included in t-T modeling allowed to establish the onset of the cooling phenomenon linked to structural growth, from west to east, at ~ 7.1-6.6 Ma (Curuyuqui-Carohuaicho), ~ 7-6.4 (Borebigua), ~ 7 Ma (Charagua), ~ 5.2 Ma (Mandeyapecua), and ~ 3-2.5 Ma (Tatarenda), from which it is inferred a slightly diachronic initial growing time for the structures of Curuyuqui-Carohuaicho, Borebigua and Charagua, and a later growth for the Mandeyapecua and Tatarenda structures with exhumation rates reaching values of ~ 1 mm/year. On the other hand, a north-to-south diachronic structural timing was identified, showing older ages concentrated at ~ 7-5 Ma for the study area to the north of Cuevo river transfer zone, and ~ 6-3.5 Ma to the south for strike-equivalent structures.

Finally, the t-T numerical modeling achieved for Devonian, Carboniferous and Miocene samples in the study area allowed to develop a quantitative analysis of the subsidence-burial and exhumation-erosion phenomena that occurred from the deposition of Silurian-Devonian source rocks to the present time, providing relevant determinations to the modeling of the Oil & Gas system in the study area. In this way, the required data for 2D and 3D petroleum system modeling was acquired and will be included in a near future contribution.

Acknowledgements

This work is the result of the integration of knowledge acquired through years of exploration in the sub-Andean fold-and-thrust belt in Bolivia and Argentina. The recent state of knowledge about the application of thermochronological data and numerical modeling for solving structural and stratigraphic situations is the result of the dedication and joint effort of professionals in the oil and gas industry and the academic system. This work was supported by YPF S.A. (Argentina) and YPFB Chaco S.A. (Bolivia). We are grateful to YPF S.A. and YPFB Chaco S.A. for their permission to publish some of the data here included. We would like to thank LA.TE. ANDES Productive and Research Center (GEOMAP-CONICET Salta Province, Argentina) for the contributions made in the application of thermochronology and the use of Andino 3D® software. We are grateful to Annika Szameitat (Czech Academy of Sciences. Prague. Czech Republic) for the (U-Th-Sm)/He data acquiring and constructive technical discussions. We would like to thank Federico Davila, Mauricio Parra, and the reviewers for providing constructive suggestions for this text.

Appendix A. Supplementary data. Supporting information.

References

Albariño, L., Dalenz Farjat, A., Alvarez, L. A., Hernández, R. M., and Perez Leyton, M. A., 2002. Las Secuencias Sedimentarias del Devónico en el Subandino Sur y el Chaco. Bolivia y Argentina. Actas 5° Congreso Exploración y Desarrollo de Hidrocarburos, Trabajos Técnicos (24 pp.) Mar del Plata, Argentina.

Alvarez, L. A., Dalenz Farjat, A., Hernández, R. M., and Albariño, L. M., 2004. Integración del análisis de líneas - tiempo, facies y biofacies como metodología de trabajo en plataformas silicoclásticas devónicas del sur de Bolivia y noroeste de Argentina. Revista de la Asociación Argentina de Sedimentología, 10(2), 103–121.

Allmendinger, R. W., Ramos, V. A., Jordan, T.E., Palma, M., Isacks, B. L., 1983. Paleogeography and Andean structural geometry, northwest Argentina: Tectonics, v. 2, p. 1–16.

Allmendinger, R. W., Zapata, T.R., 2000. The footwall ramp of the Subandean decollement, northernmost Argentina, from extended correlation of seismic reflection data: Tectonophysics, v. 321, p. 37–55.

Amidon, W. H., Luna, L. V., Fisher, G. B., Burbank, D. W., Kylander-Clark, A. R., Alonso, R., 2017. Provenance and tectonic implications of Orán Group foreland basin sediments, Río Iruya canyon, NW Argentina (23° S). Basin Research, 29, p. 96-112.

Anderson, R. B., Long, S. P., Horton, B. K., Thomson, S. N., Calle, A. Z., Stockli, D. F., 2018. Orogenic wedge evolution of the central Andes, Bolivia (21°S): Implications for Cordilleran cyclicity. Tectonics, 37. https://doi.org/10.1029/2018TC005132.

Apreda, D., D´Angiola, M., Alvarez, J. P., Vergani, G., Moreno, R., 2010. Análisis Estructural a partir de Perfiles de Buzamiento e Imágenes Resistivas en la Serranía de la Salina—Ingre, Faja Plegada y Corrida, Subandino Sur, Bolivia. XIX Congreso Geológico Boliviano, CGB, Tarija, Bolivia, accessed August 14, 2012, Disponible online en: http://www.visualcv.com_martadangiola.

Aramayo Flores, F., 1989. El cinturón plegado y sobrecorrido del norte argentino. Boletín Informaciones Petroleras Tercera: Época, v. 17, p. 2–16.

Arriagada, C., Roperch, P., Mpodozis, C., Cobbold, P. R., 2008. Paleogene building of the Bolivian Orocline: Tectonic restoration of the central Andes in 2-D map view. Tectonics, 27(6).

Baby, P., Herail G., Salinas, R.., Sempere T., 1992. Geometry and kinematic evolution of passive roof duplexes deduced from cross-section balancing: example from the foreland thrust system of the southern Bolivian Subandean zone: Tectonics, v. 11, p. 523–536.

Baby, P., Moretti I., Guillier B., Limachi, R., Mendez, E., Oller, J. and Specht M., 1995. Petroleum system of the northern and central Bolivian sub-Andean zone, in A. J. Tankard, R. Suárez S., and H. J. Welsink, Petroleum basins of South America: AAPG Memoir 62, p. 445–458.

Baby, P., Rochat, P., Mascle, G., Herail, G., 1997. Neogene shortening contribution to crustal thickening in the back arc of the central Andes: Geology, v. 25, p. 883–886.

Beltan, L., Freneix, S. Janvier, Ph., López Paulsen, O., 1987. La faune triasique de la formation de Vitiacua dans la région de Villamontes (Départment de Chuquisaca, Bolivie).- N. Jb. Geol. Paläont. Mh., 2, 99-115, Stuttgart.

Benedetto, J.L., 1991. Braquiópodos silúricos de la Formación Lipeón, flanco occidental de la Sierra de Zapla, Provincia de Jujuy, Argentina. Ameghiniana, 28 (1-2), 111- 125.

Benedetto, J.L., 2018. El Continente de Gondwana a través del Tiempo. Una Introducción a la Geología Histórica. 3era. Edición. Academia Nacional de Ciencias, Córdoba, Argentina: 1-437.

Biswas, S., Coutand, I., Grujic, D., Hager, C., Stockli, D.F., Grasemann, B, 2007. Exhumation of the Shillong plateau and its influence on east Himalayan tectonics. Tectonics 26: doi:10.1029/2007TC002125.

Brandon, M. T., 1992. Decomposition of fission-track grain-age distributions. American Journal of Science, 292(8), p. 535-564.

Brandon, M. T., 1996. Probability density plot for fission-track grain-age samples. Radiation Measurements, 26(5), p. 663-676.

Brandon, M. T., 2002. Decomposition of mixed grain age distributions using Binomfit. On track, 24(8), p. 13-18.

Capitanio, F. A., Faccenna, C., Zlotnik, S., Stegman, D. R., 2011. Subduction dynamics and the origin of Andean orogeny and the Bolivian orocline. Nature, 480(7375), p. 83-86.

Carrapa, B., DeCelles, P. G., 2015. Regional exhumation and kinematic history of the central Andes in response to cyclical orogenic processes. Geol. Soc. Am. Mem, 212, 201-213.Carvalho, I.S., 1993. Os conchostráceos fósseis das bacias interiores do Nordeste do Brasil. Tese de Doutorado. Universidade Federal do Rio de Janeiro (Programa de Pós-Graduação em Geologia). v. 1, 319 p.

Carvalho, I.S., 1996. A Conchostracofauna da Bacia de Barro (Cretáceo Inferior, Nordeste do Brasil). Anais da Academia Brasileira de Ciências, 68(4): p. 559-568.

Carvalho, I.S., 2001. Os Conchostráceos da Bacia de Cedro (Nordeste do Brasil, Cretáceo Inferior). Coleccao Chapáda do Araripere No. 1. Sumposios sobre Bacia do Araripe. p. 1-8.

Carvalho, I.S., 2014. Conchostráceos das Bacias Interiores do Nordeste Brasileiro: indicadores climáticos do Cretáceo Inferior. In: Carvalho, I.S. et al. (eds.). Paleontologia: Cenários de Vida – Paleoclimas, Interciência, Rio de Janeiro, vol. 5, p. 121-134.

Carvalho, I.S., Srivastava, N.K., 1996. Conchostraceos paleolimnadopsídeos da Bacia do Rio Nazaré (Cel. João Pessoa, Rio Grande do Norte). In: Simpósio sobre o Cretáceo do Brasil 4, Boletim, Águas de São Pedro, SP, 1996, p. 151-155.

Carvalho, I.S., Hacidume, E., Heilbron, M., 2002. Controle Tectônico na distribuição das conchostracofaunas cretáceas nas Bacias Interiores do Nordeste do Brasil. In: Simpósio sobre o Cretáceo do Brasil 6, Simpósio sobre el Cretácico de América del Sur 2, Boletim, São Pedro, São Paulo, p. 43-47.

Constantini, L. A., Schneider, F., Gutiérrez Tórrez, J. D., Esquivel Sánchez, J. R., 2018. Contribución al conocimiento estructural y en la evaluación de los sistemas petrolíferos del subandino norte de Bolivia. 10º Congreso de Exploración y Desarrollo de Hidrocarburos. Mendoza. Argentina.

Cherniak D. J. and Watson E.B., 2001. Pb diffusion in zircon. Chemical Geology 172: 5–24.

Cristallini, E., Sánchez, F., Balciunas, D., Mora, A., Ketcham, R., Nigro, J., Hernández, J., Hernández, R., 2020. Seamless low-temperature thermochronological modeling in Andino 3D, towards integrated structural and thermal simulations, Journal of South American Earth Sciences, doi: https://doi.org/10.1016/j.jsames.2020.102851.

Cruz, C.E., Sylwan, C.A., Villar, H.J., 2002. La Cuenca de Tarija, Bolivia y Noroeste de Argentina: Sistema Petrolero Único o Múltiples Sistemas Petroleros? V Congreso de Exploración y Desarrollo de Hidrocarburos. Mar Del Plata. IAPG. CD Room, 19p.

Cruz, C.E., Oller Veramendi, J., Di Benedetto, M., Pereira, M., Villar, H. 2008. Los sistemas petroleros devónicos del Subandino Sur y Pie de Monte de la Cuenca de Tarija. Bolivia. In Cruz et al., edts.: Sistemas Petroleros de las Cuencas Andinas. Instituto Argentino del Petróleo y del Gas. p. 159-187.

DeCelles, P. G., and K. Giles, 1996, Foreland basin systems: Basin Research, v. 8, p. 105–123.

DeCelles P.G., Carrapa B., Horton B.K., Gehrels G.E., 2011: Cenozoic foreland basin system in the central Andes of northwestern Argentina: Implications for Andean geodynamics and modes of deformation. Tectonics, (30), TC6013.

DeCelles, P. G., Ducea, M. N., Carrapa, B., & Kapp, P. A. (Eds.). (2015). Geodynamics of a Cordilleran Orogenic System: The Central Andes of Argentina and Northern Chile (Vol. 212). Geological Society of America.

del Papa, C., Hongn, F., Powell J., Payrola, P., Do Campo, M., Strecker, M. R., Pereyra, R., 2013. Middle Eocene-Oligocene broken-foreland evolution in the Andean Calchaqui Valley, NW Argentina: Insights from stratigraphic, structural and provenance studies: Basin Research, v. 25, no. 5, p. 574–593.

Dodson, M. H., 1973. Closure Temperature in Cooling Geochronological and Petrological Systems: Contributions to Mineralogy and Petrology 40, 259-274.

Donelick, R.A., Ketcham, R.A., Carlson, W.D., 1999. Variability of apatite fission-track annealing kinetics: II. Crystallographic orientation effects: American Mineralogist, v. 84, p. 1224-1234.

Donelick, R.A., O'Sullivan, P.B., and Ketcham, R.A., 2005. Apatite Fission-Track Analysis. Reviews in Mineralogy and Geochemistry, 58, 49–94.

Dunkl, I., 2002. Trackkey: a Windows program for calculation and graphical presentation of fission track data:Computers & Geosciences, v. 28, p. 3-12.

Dunn, J. F., Hartshorn, K.G., Hartshorn, P. W., 1995. Structural styles and hydrocarbon potential of the Subandean thrust belt of southern Bolivia, in A. J. Tankard, R. Suarez Soruco, H. J. Welsink, eds., Petroleum basins of South America: AAPG Memoir 62, p. 523–543.

Echavarria, L., Hernandez, R., Allmendinger, R., Reynolds, J., 2003. Subandean thrust and fold belt of north-western Argentina: geometry and timing of the Andean evolution. AAPG Bulletin 87: p. 965–985.

Engelder, T. M., Pelletier, J. D., 2015. Simulating foreland basin response to mountain belt kinematics and climate change in the Eastern Cordillera and Subandes: An analysis of the Chaco foreland basin in southern Bolivia. Geodynamics of a Cordilleran Orogenic System: the Central Andes of Argentina and Northern Chile. Geological Society of America, Boulder, p. 337-357.

Erikson, J., 1998. In Informe Geológico Área Entre Ríos – O'Connor – Huayco. Departamentos de Chuquisaca y Tarija. Bolivia. Informe Interno para Pluspetrol Energy. Inédito. 232 pgs. + Adjunto I + Adjunto II, Adjunto III y Anexos.

Erslev, E. A., 1991. Trishear fault-propagation folding: Geology, v. 19, no. 6, p. 617–620.

Farley, K.A., Wolf, R.A., Silver, L.T., 1996. The effects of long alpha-stopping distances on (U-Th)/He ages. Geochim Cosmochim Acta 60:4223-4229.

Farley, K.A., 2000. Helium diffusion from apatite: general behaviour as illustrated by Durango fluorapatite. Journal of Geophysical Research (Solid Earth) 105, p. 2903–2914.

Farley, K. A., 2002. (U-Th)/He Dating: Techniques, Calibrations, and Applications: Reviews in Mineralogy and Geochemistry, Noble Gases-In Geochemistry and Cosmochemistry 47, 819-844.

Flowers, R. M., Shuster, D. L., Wernicke, B. P., Farley, K. A., 2007. Radiation damage control on apatite (U–Th)/He dates from the Grand Canyon region, Colorado Plateau. Geology 35, p. 447–450.

Flowers, R.M., Ketcham, R., Shuster, D.L., Farley, K.A., 2009. Apatite (U/Th)/He thermochronometry using a radiation damage accumulation and annealing model. Geochimica et Cosmochimica Acta 73, p. 2347-2365.

Galbraith, R., 1981. On statistical models for fission track counts: Mathematical Geology, v. 13, p. 471-478.

Gallo, L. C., 2019. Evolución y formación de Pangea: su control en la sedimentación de la Cuenca de Tarija a partir de datos paleomagnéticos del sur de Bolivia (Tesis Doctoral): Universidad de Buenos Aires, 213 p.

Gephart, J. W., 1994. Topography and subduction geometry in the central Andes: Clues to the mechanics of a noncollisional orogen. Journal of Geophysical Research: Solid Earth, 99(B6), 12279-12288.

Giampaoli, P., Rojas Vera, E., 2018. Fold Growth and Lateral Linkage in the Southern Sub-Andean Fold-and-Thrust Belt of Argentina and Bolivia, p. 555-576

Giraudo, R., Limachi, R., Requena, E., Guerra, H., 1999. Geología estructural de las regiones sub-andina y piedemonte entre los 18° y 22° ¬30' S, Bolivia. Un nuevo modelo de deformación, En: IV Congreso de Exploración y Desarrollo de Hidrocarburos Acta, Mar del Plata, Argentina, Actas, p. 405–426.

Giraudo, R., Limachi, R., 2001. Pre-Silurian control in the genesis of the central and southern Bolivian fold belt: Journal of South American Earth Sciences, v. 14, no. 7, p. 665–680.

Gleadow, A. J. W., 1981. Fission-track dating methods: what are the real alternatives?. Nuclear Tracks, 5(1-2), p. 3-14.

Gleadow, A.J.W., Duddy, I.R., Green, P.F., Lovering, J.F., 1986. Confined fission track lengths in apatite: a diagnostic tool for thermal history analysis. Contrib. Mineral. Petrol. 94, 405–415.

Gleadow, A. J. W., Duddy, I. R., 1981. A natural long-term track annealing experiment for apatite. Nuclear Tracks, 5(1-2), p. 169-174.

Gleadow, A.J.W., Fitzgerald, P.G., 1987. Uplift history and structure of the Transantarctic Mountains: new evidence from fission track dating of basement apatites in the Dry Valleys area, southern Victoria Land. Earth Planet Sci. Lett. 82 (1), 1–14.

Green, P.F., Duddy, I.R., Gleadow, A.J.W., Tingate, P.R., and Laslett, G.M., 1986. Thermal annealing of fission tracks in apatite 1. Variable temperature behaviour. Chemical Geology: Isotope Geoscience Section, 59, 237–253.

Green, P.F., Duddy, I.R., Laslett, G.M., Hegarty, K.A., Gleadow, A.W., Lovering, J.F., 1989. Thermal annealing of fission tracks in apatite 4. Quantitative modelling techniques and extension to geological timescales. Chem. Geol. Isot. Geosci. 79 (2), 155–182.

Gutierrez, F., & Marshall, L. G., 1994. Los primeros huesos de dinosaurios de Bolivia. Formación Cajones (Maastrichtiano) cerca de Santa Cruz de la Sierra. Revista Técnica YPFB, 15, 131-139.

Hain, M. P., Strecker, M. R., Bookhagen, B., Alonso, R. N., Pingel, H., Schmitt, A. K., 2011. Neogene to Quaternary broken foreland formation and sedimentation dynamics in the Andes of NW Argentina (25 S). Tectonics, 30(2).

Hardy, S., Finch, E., 2007. Mechanical stratigraphy and the transition from trishear to kink-band fault-propagation fold forms above blind basement thrust faults: a discrete-element study. Marine and Petroleum Geology, 24(2), p. 75-90.

Hernández, N., Iribarne M., Apreda D., Laffitte G., and Vergani G., 2011. Nuevos conceptos estructurales a partir de la perforacion del pozo profundo Ramos xp-1012 en el Yacimiento

Ramos, Sierra de San Antonio, Provincia de Salta: VIII Congreso de Exploración y Desarrollo de Hidrocarburos, IAPG. Trabajos Tecnico, Mar del Plata, Argentina, p. 599–617.

Hernández, R. M., Echavarría, L., Allmendinger, R., Reynolds, J., Jordan, T., 2002. La Faja Plegada y Corrida Subandina del Noroeste Argentino: Secuencias Precrecimiento y Crecimiento, Geometría Estructural y Tiempo de Evolución de Los Andes: V Congreso de Exploración y Desarrollo de Hidrocarburos, Mar del Plata, CDs, Trabajos Técnicos, p. 25.

Hernandez R.M., Jordan T.E., Dalenz Farjat A., Echavarria L., Idleman B.D., Reynolds J.H., 2005. Age, Distribution, Tectonics and Eustatic Controls of the Paranense and Caribbean Marine Transgressions in Southern Bolivia and Argentina. Journal of South American Earth Sciences. 19: p. 495-512.

Hernández, R. M., Céspedes, A., Dellmans, M., Pérez Leyton, M. A., Dalenz Farjat, A., 2016. Nuevas consideraciones sobre el modelo de deformación en la Sierra de Aguaragüe: XXII Congreso Geológico de Bolivia, 6 p.

Hernández J., Cristallini, E., Hernández, R.M., Glasmacher, U., Becchio, R., Bordese, S., Rosales, A., Soria Galvarro, J., 2017. Deformational model and apatite fission-track data in a fold and thrust belt with high exhumation rates. La Lluviosa Range, Chapare. Bolivian orocline. 24th Colloquium on Latin American Earth Sciences. Heidelberg, Baden-Würtemberg, Alemania.

Hernández R. M., Hernández, J. I., Raja Gabaglia, G., Bento Freire E., Lykawka, R., Terra, G., Borges Rodrigues, E., Dalenz Farjat, A., Gallo, L., Tomezzoli, R. N., 2017. Análisis secuencial de alta frecuencia en el límite Cretácico-Paleógeno del Grupo Salta, Subcuenca de Metán, Noroeste Argentino. Estado actual y perspectivas futuras. Congreso Geológico Argentino. Relatorio, p. 1046-1079.

Hernández, J. I., 2018. Time: an Indispensable Variable to be Determined within Fold and Thrust Belts. The Sub-Andean System Case: Thermochronology and Geochronology as a possible solution. Conference paper. Geosciences Technology Workshop. AAPG. Bolivia.

Hernández, R. M., Hernández, J. I., Dalenz Farjat, A., Álvarez, L. A., Cristallini, E. O., Tomezzoli, R. N., Rosales, A., Soria Galvarro, J., 2018. Deformation and stratigraphic models of the Bolivian and Argentinean sub-Andean system: Evolution of knowledge and current trends, in G. Zamora, K. R. McClay, and V. A. Ramos, eds. Petroleum basins and hydrocarbon potential of the Andes of Peru and Bolivia: AAPG Memoir 117, p. 605–632.

Hernández, J. I, Cristallini, E., Sánchez, F., Balciunas, D., Mora, A., Ketcham, R., Nigro, J., Hernández, R., 2020. An all-in-one structural suite: Thermo-kinematic modeling applied to fault-related anticlines. The southern Sub-Andean system case: the Borebigua structure. Conference paper. AAPG Virtual Research Symposium. Andean Basins: Advances in the Geological Understanding of Fold-and-Thrust Belts of the Andes.

Horton B.K., 1998. Sediment accumulation on top of the Andean orogenic wedge: Oligocene to late Miocene basins of the Eastern Cordillera, southern Bolivia. GSA Bulletin, 110(9): 1174-1192.

Horton, B. K., 2018. Tectonic regimes of the central and southern Andes: Responses to variations in plate coupling during subduction. Tectonics, 37(2), p. 402-429.

Hurford, A.J., Green, P.F., 1982. A users' guide to fission track dating calibration: Earth and Planetary Science Letters, v. 59, p. 343-354.

Hurford, A.J., Green, P.F., 1983. The zeta age calibration of fission-track dating: Chemical Geology, v. 41, p. 285-317.

Kennan L., Lamb S., Rundle C., 1995. K-Ar dates from the Altiplano and Cordillera Oriental of Bolivia: implications for Cenozoic stratigraphy and tectonics. Journal of South American Earth Sciences: 8(2): 163-186.

Ketcham, R.A., 2005. Forward and Inverse Modeling of Low-Temperature Thermochronometry Data: Reviews in Mineralogy and Geochemistry, v. 58, p. 275-314.

Ketcham, R.A., Carter, A., Donelick, R.A., Barbarand, J., Hurford, A.J., 2007a. Improved measurement of fission-track annealing in apatite using c-axis projection: American Mineralogist, v. 92, p. 789-798.

Ketcham, R.A., Carter, A., Donelick, R.A., Barbarand, J., Hurford, A.J., 2007b. Improved modeling of fission-track annealing in apatite: American Mineralogist, v. 92, p. 799-810.

Ketcham, R.A., Donelick, R.A., Balestrieri, M.L., Zattin, M., 2009. Reproducibility of apatite fission-track length data and thermal history reconstruction: Earth and Planetary Science Letters, v. 284, p. 504-515.

Ketcham, R.A., 2017. HeFTy Version 1.9.3, Manual.

Kley, J., 1996, Transition from basement-involved to thinskinned thrusting in the Cordillera Oriental of southern Bolivia: Tectonics, v. 15, p. 763–775.

Kley, J., Gangui, A. H., Krugger, D., 1996. Basement involved blind thrusting in the eastern Cordillera Oriental, southern Bolivia: Evidence from cross-sectional balancing, gravimetric and magnetotelluric data: Tectonophysics, v. 259, p. 171–184.

Kley, J., Monaldi, C. R., 1999. Estructura de las Sierras Subandinas y del Sistema de Santa Bárbara: Salta, Argentina, Congreso Geológico Argentino, p. 415–425.

Kley, J., Monaldi, C. R., 2002. Tectonic inversion in the Santa Barbara System of the central Andean foreland thrust belt, northwestern Argentina. Tectonics, 21(6), p. 11-1.

Kusiak, M.E., Mascle, G., Ramos, V.A. 2014. El Magmatismo Mesozoico asociado a los procesos extensionales en las Cuencas de Rift del Subandino Boliviano y la importancia de su ubicación geocronológica en paleogeografía de América del Sur. Memorias del Congreso Argentino de Hidrocarburos, Mendoza. 20 p.

Lamb S., Hoke, L., 1997. Origin of the high plateau in the Central Andes, Bolivia, South America. Tectonics, 16(4): p. 623-649.

Lee J.K.W., 1997. Pb, U, and Th diffusion in natural zircon. Nature 390: 159–162.

Leturmy, P., Mugnier, J. L., Vinour, P., Baby, P., Colletta, B., Chabron, E., 2000. Piggyback basin development above a thin-skinned thrust belt with two detachment levels as a function of interactions between tectonic and superficial mass transfer: the case of the Subandean Zone (Bolivia). Tectonophysics, 320(1), p. 45-67.

Ludwig K.R., 2003. User's Manual Isoplot 3.00. A Geochronological Toolkit for Microsoft Excel. Geochronology Center Special Publication 4. Berkeley.

Ludwig, K.R., 2008. Manual for Isoplot 3.7: Berkeley Geochronology Center, Special Publication No. 4. rev. August 26, 2008, 77 pp.

Marshall, L.G. and Sempere, T., 1991. The Eocene to Pleistocene vertebrates of Bolivia and their stratigraphic context, a review. In R. Suárez-Soruco (ed.). Fósiles y Facies de Bolivia, Rev. Téc. YPFB, Santa Cruz, 12 (3-4), p. 631-652.

Mingramm, A., Russo, A. 1969. Sierras Subandinas y Chaco Salteno, in A. F. Leanza, ed., Geología Regional Argentina: Academia Nacional de Ciencias de Córdoba, p. 185–211.

Mingramm, A., Russo, A., Pozzo, A., Cazau, L., 1979. Sierras Subandinas, in J. C. M. Turner, ed., Geología Regional Argentina (Vol. 1): Cordoba, Academia Nacional de Ciencias, p. 95-138.

Mombrú, C., and F. Aramayo Flores, 1986. Geología del Yacimiento Aguaragüe. Boletín Informaciones Petroleras: Tercera Época, v. 6, p. 53–64.

Moretti, I., Labaume, P., Sheppard, S., Boulhgue, J., 2002. Compartmentalisation of the migration pathways in the Sub-Andean Zone, Bolivia Proceeding of Geofluid 2000, Barcelona: Tectonophysics, v. 348, p. 5–24.

Mulch, A., Uba, C. E., Strecker, M. R., Schoenberg, R., Chamberlain, C. P., 2010. Late Miocene climate variability and surface elevation in the central Andes. Earth and Planetary Science Letters, 290(1-2), p. 173-182.

Oller-Veramendi, J., Franco, A., 1981. Informe geológico final. Anticlinal de Terebinto.- Informe interno YPFB (GXG-2923), Santa Cruz, diciembre 1981.

Pearson, D. M., Kapp, P., DeCelles, P. G., Reiners, P. W., Gehrels, G. E., Ducea, M. N., Pullen, A., 2013. Influence of pre-Andean crustal structure on Cenozoic thrust belt kinematics and shortening magnitude: Northwestern Argentina. Geosphere, 9(6), p. 1766-1782.

Quade, J., et al., 2015. The growth of the central Andes, 22 S–26 S. Geol Soc Am Mem, 12, p. 277-308.

Reiners, P., Brandon, M., 2006. Using Thermochronology to understand orogenic erosion. Annu. Rev. Earth Planet Sci. 34 (1), 419–466. https://doi.org/10.1146/annurev. earth.34.031405.125202.

Renne, P.R., Ernesto, M., Pacca, I.I.G., Coe, R.S., Glen, J.M., Prévot, M., Perrin, M., 1992. The age of Paraná flood volcanism, rifting of Gondwanaland, and the Jurassic-Cretaceous boundary. Science 258, 975–979.

Renne, P.R., Deckart, K., Ernesto, M., Féraud, G., Piccirillo, E.M., 1996. Age of Ponta Grossa dike swarm (Brazil), and implications to Parana flood volcanism. Earth Planet. Sci. Lett. 144 199-21.

Rocha, E., 2013. Estilos estructurales del Subandino Sur de Bolivia (Tesis Doctoral): Universidad de Buenos Aires, 204 p., accessed March 5, 2018, http://digital.bl.fcen.uba.ar/ Download/Tesis/Tesis_5476_Rocha.pdf.

Rocha, E., and E. O. Cristallini, 2018. Controls on thrusts spacing: An example from the subandean fold and thrust belt of southern Bolivia, in G. Zamora, K. R. McClay, and V. A. Ramos, eds., Petroleum basins and hydrocarbon potential of the Andes of Perú and Bolivia: AAPG Memoir 117, p. 457–474.

Rosario, J., Jordan, T. E., Garzione, P., Hernández, J. I., Hernández, R. M., Higgins, P., 2008. Estratigrafía de paleosuelos y sus implicancias paleoclimáticas en el noroeste argentino. XVII Congreso Geológico Argentino. Jujuy.

Rosario, J., Jordan, T. E., Garzione, P., Higgins, P., Hernández, J. I., Hernández, R. M., 2017. Condiciones paleoclimáticas del Mioceno-Plioceno temprano en el Chaco Occidental del Noroeste argentino. XX Congreso Geológico Argentino. Tucumán.

Rousse, S. 2018. Future exploration potential associated with to glaciogenic carboniferous series in Bolivian Subandean Chaco Foreland System. Geosciences Technology Workshop Conference. AAPG. Santa Cruz de la Sierra, Bolivia.

Rousse, S., Gilder, S., Fornari, M., Sempere, T., 2005. Insight into the Neogene tectonic history of the northern Bolivian Orocline from new paleomagnetic and geochronologic data. Tectonics, 24(6).

Sánchez, Á., Goncalves, Ana. M.., Asquith, K., Hill, K., 2020. Kinematic deformation model of the south-central subandean zone, Bolivia, Journal of South American Earth Sciences, doi: https://doi.org/10.1016/j.jsames.2020.102768.

Starck, D., Constantini, L., Schulz, A., 2002. Análisis de algunos aspectos geométricos y evolutivos de las estructuras de la faja plegada Subandina del norte de Argentina y el sur de Bolivia, in V Congreso de exploración and Desarrollo de Hidrocarburos: Mar del Plata, Argentina, Trabajos técnicos, 15 p.

Schneider F., Constantini L., Mayta R., Rousse S., Esquivel J., 2018. Contribución a la evaluación del potencial petrolífero del subandino sur de Bolivia. 10º Congreso de Exploración y Desarrollo de Hidrocarburos. Mendoza. Argentina.

Scotese, C.R., Golonka, J., 1992. Paleogeographic Atlas. Paleomap Projekt. Department of Geology, U. Texas at Arlington.

Scotese, C.R., Boucot, A.J., McKerrow, W.S., 1999. Gondwanan paleogeography and paleoclimatology. J. Afr. Earth Sci. 28 (1), 99–114.

Sempere, T., Butler, R. F., Richards, D. R., Marshall, L. G., Sharp, W., Swisher Iii, C. C., 1997. Stratigraphy and chronology of Upper Cretaceous–lower Paleogene strata in Bolivia and northwest Argentina. Geological Society of America Bulletin, 109(6), p. 709-727.

Sempere, T., Carlier, G., Carlotto, V., Jacay, J., 1998. Rifting Pérmico Superior – Jurásico Medio en la Cordillera Oriental de Perú y Bolivia. XIII Congreso Geológico Boliviano, Potosí, 1998: 8 pgs.

Shuster, D.L., Flowers, R.M. y Farley, K.A., 2006. The influence of natural radiation damage on helium diffusion kinetics in apatite. Earth Planet. Sci. Lett. 249, p. 148–161.

Siks, B. C., & Horton, B. K., 2011. Growth and fragmentation of the Andean foreland basin during eastward advance of fold-thrust deformation, Puna plateau and Eastern Cordillera, northern Argentina. Tectonics, 30(6).

Starck, D., Constantini, L., Schulz, A., 2002. Análisis de algunos aspectos geométricos y evolutivos de las estructuras de la faja plegada Subandina del norte de Argentina y el sur de Bolivia, in V Congreso de exploración and Desarrollo de Hidrocarburos: Mar del Plata, Argentina, Trabajos técnicos, 15 p.

Stockli D.F., Dumitru T.A., McWilliams M.O., Farley K.A., 2003. Cenozoic tectonic evolution of the White Mountains, California and Nevada. Geological Society of America Bulletin 115: 788-816.

Strecker, M. R., Cerveny, P., Bloom, A. L., Malizia, D., 1989. Late Cenozoic tectonism and landscape development in the foreland of the Andes: Northern Sierras Pampeanas (26°–28°S), Argentina: Tectonics, v. 8, p. 517–534.

Strecker, M. R., Hilley, G. E., Bookhagen, B., Sobel, E. R., 2012. Structural, geomorphic and depositional characteristics of contiguous and broken foreland basins: Examples from the eastern flanks of the central Andes in Bolivia and NW Argentina. In C. Busby & A. Azor (Eds.), Tectonics of sedimentary basins: Recent advances (pp. 508–521). Chichester, UK: Wiley-Blackwell.

Suárez Riglos, M. and Dalenz Farjat, A., 1993. Pteriomorphia (Bivalvia) Noriano de la Formación Vitiacua, del área de Villamontes (Tarija). In R. Suárez-Soruco (ed.). Fósiles y Facies de Bolivia, Vol. II - Invertebrados y Paleobotánica). Revista Técnica de YPFB, 13/14 (1-4), 155-160.

Suarez Riglos M., De Souza Carvalho I., 2018. Conchostracos cretácicos de la Formación Castellón, Subandino sur de Bolivia, in: M. Suárez Riglos, A. Dalenz Farjat, and M. A. Pérez Leyton , eds. Fósiles y Facies de Bolivia, p.114-123.

Suarez Soruco, R., and J. Lobo Boneta, 1983. La fase compresiva eohercínica en el sector oriental de la cuenca cordillerana de Bolivia. Presentación del Mapa Paleogeológico Pre-Formación Tupambi (Namuriano) elaborado en base a información palinológica.- Revista Técnica de YPFB, 9 (1-4): p. 189-202, La Paz.

Troth, I., Marshall, J.E.A., Racey, A., Becker, R.T., 2011. Devonian sea-level change in Bolivia: A high palaeolatitude biostratigraphical calibration of the global sea-level curve. Palaeogeography, Palaeoclimatology, Palaeoecology 304: 3-20.

Uba, C. E., Strecker, M. R., Schmitt, A. K., 2007. Increased sediment accumulation rates and climatic forcing in the central Andes during the late Miocene. Geology, 35(11), p. 979-982.

Uba, C. E., Kley, J., Strecker, M. R., Schmitt, A. K., 2009. Unsteady evolution of the Bolivian Subandean thrust belt: The role of enhanced erosion and clastic wedge progradation. Earth and Planetary Science Letters, 281(3-4), p. 134-146.

Vermeesch, P., Seward, D., Latkoczy, C., Wipf, M., Gunther, D., Baur, H., 2007. Alpha-emitting mineral inclusions in apatite, their effect on (U–Th)/He ages, and how to reduce it. Geochim. Cosmochim. Acta 31, 1737–1746.

Viera, A., Hernández, R.M., (2001). Carboniferous Stratigraphic Analysis in the Subandean Foothills and the Chaco Plains of Tarija Basin-Bolivia. AAPG Convention, Denver 2001, 12pp.

Wagner, G.A., Van den Haute, P., 1992. Fission-track dating: Stuttgart, Enke Verlag - Kluwer Academic Publishers.

Wipf M.A., 2006. Evolution of the Western Cordillera and coastal margin of Peru: evidence from low-temperature thermochronology and geomorphology ETH, Zürich, pp 152.

Wolf, R.A., Farley, K.A., Silver, L.T., 1996. Helium diffusion and low-temperature thermochronometry of apatite. Geochim. Cosmochim. Acta 60, 4231-4240.

Wygrala, B. P., 1989. Integrated study of an oil field in the Southern Po Basin. Northern Italy, 328.

Zapata, T. R., Zamora, G., Ansa, A., Varade, R., 2005. Geometry and structural controls of fault-related folds from the Andes: Examples from petroleum provinces of Bolivia and

Argentina: international conference on theory and application of fault related folding in foreland basins, resúmenes digitales. p. 76–77. RIPED, Beijing, China.

Zubieta Rossetti, D., Baby, P., Mugnier, J. L., 1996. Cenozoic evolution of the Andean foreland basin between 15°30’ and 22°00’S. 3nd. Symposium International Géodynamique Andine, St Malo (France): p. 529-532.

Multiple thermochronometers applied to the quantitative analysis of compressive systems: the southern sub-Andean fold and thrust belt of Bolivia. From source rock to trap

Highlights

1) The evolution of fold and thrust belt systems requires time data restrictions.

2) Multiple thermochronometers integration for characterizing compressive systems.

3) Time-Temperature trajectories leading to structural and stratigraphic definitions.

4) The sub-Andean system dynamics defined through thermochronological analysis.

5) Oil and Gas system variables through thermochronology in the sub-Andean system.

Declaration of interests

☒ The authors declare that they have no known competing financial interests or personal relationships that could have appeared to influence the work reported in this paper.

☐The authors declare the following financial interests/personal relationships which may be considered as potential competing interests: